CYCLOPs: A Unified Framework for Surface Flux-Driven Cyclones Outside the Tropics

Kerry Emanuel (1), Tommaso Alberti (2), Stella Bourdin (3), Suzana J. Camargo (4), Davide Faranda (5,6,7), Manos Flaounas (8,9), Juan Jesus Gonzalez-Aleman (10), Chia-Ying Lee (4), Mario Marcello Miglietta (11), Claudia Pasquero (12), Alice Portal (13), Hamish Ramsay (14), Marco Reale (15), Romualdo Romero (16)

(1) Massachusetts Institute of Technology, 77 Mass. Ave., Cambridge, MA 02139

(2) Istituto Nazionale di Geofisica e Vulcanologia, Rome, Italy

(3) Atmospheric, Oceanic and Planetary Physics, Department of Physics, University of Oxford, Oxford, United Kingdom

(4) Lamont-Doherty Earth Observatory, Columbia University, Palisades, New York, USA

(5) Laboratoire des Sciences du Climat et de l'Environnement, UMR 8212 CEA-CNRS-UVSQ, Université Paris-Saclay & IPSL, CE Saclay l'Orme des Merisiers, 91191 Gif-sur-Yvette, France

(6) London Mathematical Laboratory, 8 Margravine Gardens, London W6 8RH, UK

(7) LMD/IPSL, ENS, Université PSL, École Polytechnique, Institut Polytechnique de Paris, Sorbonne Université, CNRS, Paris France

(8) Institute for Atmospheric and Climate Science, ETH Zurich, Zurich, Switzerland

(9) Institute of Oceanography, Hellenic Centre for Marine Research, Athens, Greece

(10) CNR-ISAC, Padua, Italy

(11) Spanish State Meteorological Agency, AEMET, Department Development and Applications

(12) Department of Earth and Environmental Sciences, University of Milano - Bicocca, Italy

(13) Institute of Atmospheric Sciences and Climate (CNR-ISAC), National Research Council of Italy, Bologna, Italy

(14) CSIRO Environment, Aspendale, Victoria, Australia

(15) National Institute of Oceanography and Applied Geophysics - OGS, Trieste, Italy

(16) Grup de Meteorologia, Departament de Física, Universitat de les Illes Balears, Palma de Mallorca, Spain

Correspondence: Kerry Emanuel (emanuel@mit.edu)

29   Abstract

30   Cyclonic storms resembling tropical cyclones are sometimes observed well outside the tropics.
31   These include medicanes, polar lows, subtropical cyclones, Kona storms, and possibly some
32   cases of Australian East Coast cyclones. Their structural similarity to tropical cyclones lies in
33   their tight, nearly axisymmetric inner cores, eyes, and spiral bands. Previous studies of these
34   phenomena suggest that they are partly and sometimes wholly driven by surface enthalpy
35   fluxes, as with tropical cyclones. Here we show, through a series of case studies, that many of
36   these non-tropical cyclones have morphologies and structures that resemble each other and
37   also closely match those of tropical transitioning cyclones, with the important distinction that the
38   potential intensity that supports them is not present in the pre-storm environment but rather is
39   locally generated in the course of their development. We therefore propose to call these storms
40   CYClones from Locally Originating Potential intensity (CYCLOPs). We emphasize that mature
41   cyclops are essentially the same as TCs but their development requires substantial modification
42   of their thermodynamic environment on short time scales. Like their tropical cousins, the rapid
43   development and strong winds of cyclops<s>CYCLOP</s>s pose a significant threat and forecast
44   challenge for islands and coastal regions.

45   # 1.   Introduction

46   Cyclones that resemble tropical cyclones are occasionally observed to develop well outside the
47   tropics. These include polar lows, medicanes, subtropical cyclones, Kona storms (central North
48   Pacific), and perhaps some cases of Australian East Coast cyclones. The identification of such
49   systems is usually based on their appearance in satellite imagery and on the environmental
50   conditions in which they occur. Here we show that many of these systems are manifestations of
51   the same physical phenomenon and, as such, should be given a common, physically-based
52   designation. We propose to call these CYClones from Locally Originating Potential intensity
53   (CYCLOPs), with reference to the one-eyed creatures of Greek mythology[1]. We show that in
54   many respects these developments resemble classical "tropical transition" (TT) events (e.g.
55   Bosart and Bartlo, 1991), but they are distinguished from the latter by occurring in regions
56   where the climatological potential intensity is small or zero. (Some events previously identified
57   as TT events were probably examples of cyclops.) Their often rapid development and intense
58   mesoscale inner cores, compared to extratropical cyclones, make cyclops significant hazards
59   and a forecasting challenge.

60   Cyclones of synoptic and sub-synoptic scale are powered by one or both of two energy sources:
61   the available potential energy (APE) associated with isobaric temperature gradients
62   (baroclinity), and fluxes of enthalpy (sensible and latent heat) from the surface (usually the

---

[1] Late in the process of writing this paper, we discovered that there is a scientific research project by the same name, standing for "Improving Mediterranean CYCLOnes Predictions in Seasonal forecasts with artificial intelligence" (https://www.cmcc.it/projects/cyclops-improving-mediterranean-cyclones-predictions-in-seasonal-forecasts-with-artificial-intelligence). Its team leader, Leone Cavicchia, has graciously agreed with our use of the same name.

63 ocean) to the atmosphere[2]. A normal extratropical cyclone over land is an example of the
64 former, while the latter is epitomized by a classical tropical cyclone. Extratropical transitioning
65 and tropical transitioning cyclones[3] are powered by both sources, with the relative proportion
66 usually varying over the life of the storm. Additionally, we note that tropical cyclones often
67 originate in disturbances, such as African easterly waves, that derive their energy from ~~isobaric~~
68 ~~temperature gradients.~~ baroclinic and barotropic sources.

69 Like tropical cyclones, cyclops are mainly powered by surface enthalpy fluxes, but differ from
70 the former in that the required potential intensity is produced locally and transiently, ~~by~~
71 ~~baroclinic processes,~~ whereas tropical cyclones develop in seasons and regions where
72 sufficient potential intensity is always present. Cyclops closely resemble the strongly baroclinic
73 cases of tropical transition defined and discussed by Davis and Bosart (2004), except that they
74 occur in regions where the climatological potential intensity is too small for tropical cyclogenesis,
75 relying on synoptic-scale perturbations that locally enhance potential intensity in space and
76 time. Davi~~se~~s and Bosart (2004) confined their attention to tropical cyclone formation in regions
77 of high sea surface temperature, stating that "The precursor cyclone must occlude and remain
78 over warm water (≳26°C) for at least a day following occlusion." Similarly, McTaggart-Cowan et
79 al. (2008) and McTaggart-Cowan et al. (2013) only examined cases of tropical transition that
80 resulted in named tropical cyclones. But McTaggert-Cowan et al. (2015) recognized that around
81 5% of the cases they identified as tropical transition cases occurred over colder water and that
82 upper-level troughs played a key role in destabilizing the atmosphere with respect to the sea
83 surface. We here build on this work and place it within the framework of potential intensity
84 theory.

85 The basic physics of cyclops was explored by the first author in reference to medicanes, and is
86 illustrated in Figure 1. While the actual evolution is, of course, continuous, it is simpler to
87 discuss it in phases. For this narrow purpose, we assume that a cut-off cyclone has already
88 formed in the upper troposphere, signified by the presence of ~~In the first phase (Figure 1a),~~
89 ~~Rossby wave breaking has resulted in~~ an isolated potential vorticity (PV) anomaly near the
90 tropopause (Figure 1a). We idealize this anomaly as circularly symmetric and show a cross-
91 section through it; in practice, such developments are seldom close to axisymmetric in their
92 earlier stages~~.~~ In the illustration, the first phase is assumed to occur over land, but that need not
93 be the case in general.

---

[2] Some would regard latent heating as an additional energy source, but condensation through a deep layer is present in most cyclones and, being strongly tied to vertical motion, should not be regarded as an external heat source but rather as a modification of the ~~effective~~ static stability (Emanuel et al., 1994).

[3] Extratropical transitioning cyclones are storms whose energy source is transitioning from surface fluxes to ambient baroclinity, while the energy source of tropical transitioning cyclones is moving in the opposite direction.
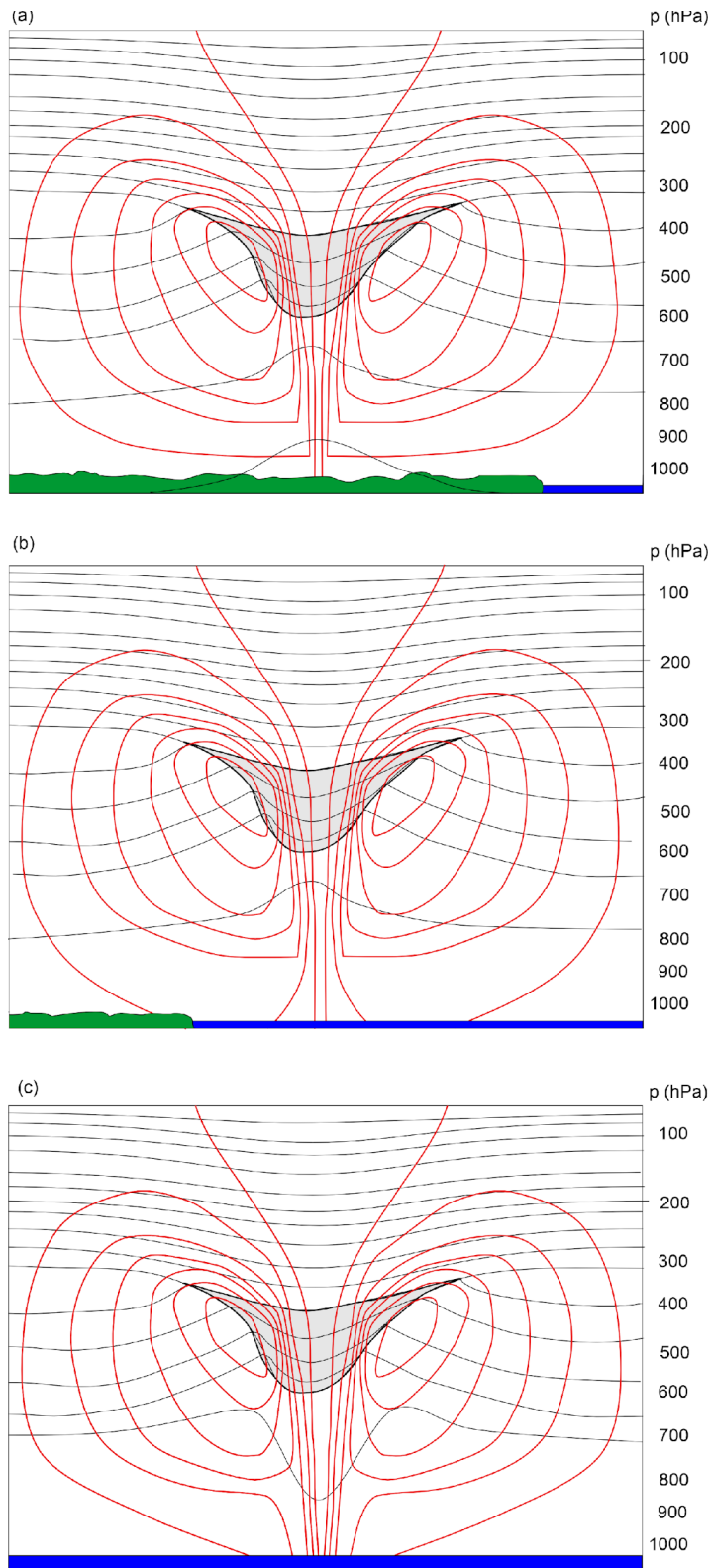
Figure 1: Three stages in the development of a cyclop. Each of the three panels shows a cross-section through a~~n~~ ~~circular,~~ isolated PV anomaly at the tropopause (gray shading), idealized as circular. The thin black curves are isentropes, while the red curves are isotachs of the flow normal to the cross-section. In the first phase (a), the PV anomaly is over land, the troposphere beneath it is anomalously cold, and there may be no flow at the surface. The system moves out over open water in the next phase (b) and warming of the boundary layer and lower troposphere suffices to eliminate the cold anomaly at and near the surface. Weak cyclonic flow develops in response to the positive PV anomaly aloft. In the final phase (c), the surface heat fluxes become important and a tight, inner warm core develops.

94

95   During the creation of the near-tropopause PV anomaly, some combination of lifting and cold air
96   seclusion has cooled and ~~moistened~~ humidified the column underneath the PV anomaly, and
97   the cold anomaly extends right to the surface. From a PV inversion perspective, the near-
98   surface anticyclone that results from inverting the negative potential temperature anomaly at the
99   surface is assumed to just cancel the cyclonic anomaly that results from inverting the
100   tropopause PV anomaly, yielding no circulation at the surface. This assumption is made for
101   simplicity here and we do not mean to imply that such a cancellation is common.

102   In phase 2 (Figure 1b), the system drifts out over open water that is warm enough to diminish
103   and eventually eliminate the cold anomaly at the surface, "unshielding" it from the PV anomaly
104   aloft. During this phase, a cyclonic circulation develops in the lower troposphere, with a
105   horizontal scale commensurate with that of the PV anomaly.

106   If the local potential intensity is now large enough, and the air aloft sufficiently close to
107   saturation, Wind-Induced Surface Heat Exchange (WISHE) can develop a tropical cyclone-like
108   vortex (phase3, Figure 1c), with a warm inner core, eye and eyewall, and perhaps spiral bands.
109   Note that the inner core may be warm only with respect to the synoptic-scale cold anomaly
110   surrounding it, not necessarily with respect to the distant environment. At mid-levels, the
111   temperature anomaly may manifest as a small-scale warm anomaly surrounded by a synoptic-
112   scale cold anomaly.

113   In reality, these phases blend together into a continuum. Moreover, all three phases may (and
114   often do) occur over water. One practical challenge is calculating the potential intensity. This
115   should be calculated using the temperatures of the sea surface and the free troposphere under
116   the PV anomaly aloft, but before the troposphere has appreciably warmed from surface fluxes.
117   In practice, because the warming occurs either as the PV anomaly develops over water, or as it
118   moves over water from land, we have no access to the sounding of the free troposphere *before*
119   it has warmed up. The true potential intensity for a TC developing within the cold column under
120   the PV anomaly is hence impossible to obtain. Nevertheless, we can estimate how cold the
121   troposphere was before surface fluxes warmed it by assuming that the troposphere has an
122   approximately moist adiabatic temperature profile and using the upper tropospheric geopotential
123   height in the cold cutoff cyclone to estimate the negative temperature perturbation underneath it.
124   This was done in Emanuel (2005), and a slightly improved version is derived in the Appendix.
125   The result is a modified potential intensity, V_{pm}, given by

$$V_{pm}^2 = V_p^2 - \frac{C_k}{C_D}\frac{T_s}{T_{400}}\phi_{400}',$$ (1)

127   where V_p is the potential intensity calculated in the usual way from the local sea surface

128   temperature and atmospheric sounding, ϕ_{400}' is the perturbation away from climatology of the

129   upper tropospheric geopotential, which we here evaluate at 400 hPa, ~~away from climatology~~,

130   C_k and C_D are the surface exchange coefficients for enthalpy and drag, and T_s and T_{400} are

131   the absolute temperatures at the surface and 400 hPa. In what follows, we approximate the

132 coefficient multiplying ϕ'_{400} in (1) by a constant value, 1.3, a reasonable estimate of the mean
133 value of the coefficient.

134 Beginning with an upper cold cyclone in an environment of otherwise zero potential intensity,
135 Emanuel (2005) simulated the development of a WISHE-driven cyclone using the axisymmetric,
136 nonhydrostatic hurricane model of Rotunno and Emanuel (1987). The cold, moist troposphere
137 under such an upper cyclone proves to be an ideal incubator of surface flux-driven cyclones
138 with characteristics nearly identical to those of tropical cyclones. One interesting facet of the
139 process is that the anomalous surface enthalpy flux destroys the parent upper cold low over a
140 period of a few days, through the action of deep convection. This in another way in which
141 cyclops are distinguished from tropical cyclones, which tap spatially extensive regions of high
142 potential intensity.

2.   Why it matters

144 Why should we care whether a cyclone is driven by surface fluxes or baroclinity? From a
145 practical forecasting standpoint, the spatial distributions of weather hazards, like rain and wind,
146 can be very different, as can be the development time scales and fundamental predictability.

147 In classical baroclinic cyclones, the strongest winds are often found in frontal zones and can be
148 far from the cyclone center, while and precipitation is usually heaviest in these frontal zones and
149 in a shield of slantwise ascent extending poleward from the surface cyclone. There is long
150 experience in forecasting baroclinic storms, and today's numerical weather prediction (NWP) of
151 these events has become quite accurate, even many days ahead. Importantly, baroclinic
152 cyclones are well resolved by today's NWP models. While baroclinic cyclones can intensify
153 rapidly, both the magnitude and timing of intensification are usually forecast accurately, and
154 uncertainties are well quantified by NWP ensembles.

155 By contrast, the physics of tropical cyclone intensification, involving a positive feedback between
156 surface winds and surface enthalpy fluxes, results in an intense, concentrated core with high
157 winds and heavy precipitation (which can be snow in the case of polar lows). The eyewalls of
158 surface flux-driven cyclones are strongly frontogenetical (Emanuel, 1997), further concentrating
159 wind and rain in an annulus of mesoscale dimensions. The intensity of surface flux-driven
160 cyclones can change very rapidly and often unpredictably, presenting a severe challenge to
161 forecasters. For example, Hurricane Otis of 2023 intensified from a tropical storm to a Category
162 5 hurricane in about 30 hours, devastating Acapulco, Mexico, with little warning from
163 forecasters. The small size of the core of high winds and heavy precipitation means that small
164 errors in the forecast position of the center of the storm can lead to large errors in local wind and
165 precipitation predictions. Surface flux-driven cyclones are too small to be well resolved by
166 today's global NWP models, and even if they were well resolved, fundamental predictability
167 studies show high levels of intrinsic unpredictability of rapid intensity changes (Zhang et al.,
168 2014).

169 The time and space scales of surface flux-driven cyclones are such that they couple strongly
170 with the ocean, producing near-inertial currents whose shear-driven turbulence mixes to the

171 surface generally (but not always) colder water from below the surface mixed layer. This has an
172 important (usually negative) feedback on the intensification of such cyclones. Accurate
173 numerical forecasting of surface flux-driven cyclones therefore requires an interactive ocean,
174 generally missing from today's NWP models because it is not very important for baroclinic
175 cyclones and because of the additional computational burden.

176 For these reasons, it matters (or should matter) to forecasters whether a particular development
177 is primarily driven by surface fluxes or by ambient baroclinity. The structural differences
178 described above are often detectable in satellite imagery; at the same time, such imagery is
179 sometimes misleading about the underlying physics. For example, classical baroclinic
180 development sometimes develops cloud-free eyes surrounded by convection through the warm
181 seclusion process, even over land, and yet may not have the intense annular concentration of
182 wind and rain characteristic of surface flux-driven cyclones (Tous and Romero, 2013).

183 ~~Armed with the conceptual cyclop model developed in section 1 and modified potential intensity~~
184 ~~given by (1), we now turn to case studies of the development of medicanes, polar lows, a~~
185 ~~subtropical cyclone, and a Kona storm, showing that the dynamic and thermodynamic pathways~~
186 ~~are similar. Specifically, each case developed after the formation of a deep, cold-core cut-off~~
187 ~~cyclone in the upper troposphere that often resulted from a Rossby wave breaking event. The~~
188 ~~lifting of the tropospheric air in response to the developing potential vorticity anomaly near the~~
189 ~~tropopause created a deep, cold, and presumably humid column. The deep cold air over bodies~~
190 ~~of relatively warmer water substantially elevates potential intensity, while its high relative~~
191 ~~humidity discourages evaporatively driven convective downdrafts, which tamp down the needed~~
192 ~~increase in boundary layer enthalpy. Low vertical wind shear near the core of the cutoff cyclone,~~
193 ~~coupled with high potential intensity and humidity, provide an ideal embryo for tropical cyclone-~~
194 ~~like development.~~

195 ~~In what follows we focus on the cutoff cyclone evolution and the development of modified~~
196 ~~potential intensity. In a particular case, we compare reanalysis column water vapor to that~~
197 ~~estimated from satellite measurements. The differences between these are significant enough~~
198 ~~to cast some doubt on the quality of reanalyzed water vapor associated with the small-scale~~
199 ~~cyclop developments, thus we do not focus on water vapor even though it is known to be~~
200 ~~important for intensification of tropical cyclones.~~

201 ~~We also examined, but do not show here, several cases of Australian East Coast Lows (Holland~~
202 ~~et al., 1987). Owing to the East Australian Current, the climatological potential intensity is~~
203 ~~substantial off the southeast coast of Australia, and the cyclop developments we analyzed~~
204 ~~behaved more like classical tropical transitions, with little or no role of the synoptic scale~~
205 ~~dynamics in enhancing the existing potential intensity. We suspect that there may be other~~
206 ~~cases in which the latter process was important, but did not conduct a search for such cases. It~~
207 ~~is clear that in many of these cases surface heat fluxes were important in driving the cyclone~~
208 ~~(Cavicchia et al., 2019). We also examined a small number of subtropical cyclones that~~
209 ~~developed in the South Atlantic, but as with the Australian cases, they resembled classical~~
210 ~~tropical transitions, though again we suspect there may be cyclop cases there as well.~~

3. Case Studies

214 Armed with the conceptual cyclop model developed in section 1 and modified potential intensity
215 given by (1), we now turn to case studies of the development of medicanes, polar lows, a
216 subtropical cyclone, and a Kona storm, showing that the dynamic and thermodynamic pathways
217 are similar. Specifically, each case developed after the formation of a deep, cold-core cut-off
218 cyclone in the upper troposphere that often resulted from a Rossby wave breaking event. The
219 lifting of the tropospheric air in response to the developing potential vorticity anomaly near the
220 tropopause created a deep, cold, and presumably humid column. The deep cold air over bodies
221 of relatively warmer water substantially elevates potential intensity, while its high relative
222 humidity discourages evaporatively driven convective downdrafts, which tamp down the needed
223 increase in boundary layer enthalpy. Low vertical wind shear near the core of the cutoff cyclone,
224 coupled with high potential intensity and humidity, provide an ideal embryo for tropical cyclone-
225 like development. The requirement for low vertical wind shear may prevent open troughs from
226 producing cyclops, event if the potential intensity is elevated.

227 In what follows we focus on the cutoff cyclone evolution and the development of modified
228 potential intensity. In a particular case, we compare reanalysis column water vapor to that
229 estimated from satellite measurements. The differences between these are significant enough
230 to cast some doubt on the quality of reanalyzed water vapor associated with the small-scale
231 cyclop developments, thus we do not focus on water vapor even though it is known to be
232 important for intensification of tropical cyclones.

233 We also examined, but do not show here, several cases of Australian East Coast Lows (Holland
234 et al., 1987). Owing to the East Australian Current, the climatological potential intensity is
235 substantial off the southeast coast of Australia, and the cyclop developments we analyzed
236 behaved more like classical tropical transitions, with little or no role of the synoptic scale
237 dynamics in enhancing the existing potential intensity. We suspect that there may be other
238 cases in which the latter process was important, but did not conduct a search for such cases. It
239 is clear that in many of these cases surface heat fluxes were important in driving the cyclone
240 (Cavicchia et al., 2019). We also examined a small number of subtropical cyclones that
241 developed in the South Atlantic, but as with the Australian cases, they resembled classical
242 tropical transitions, though again we suspect there may be cyclop cases there as well.

243 As with tropical cyclones, there are variations on the theme of cyclops, and we explore these in
244 the closing sections.

3.1 Medicane Celano of January, 1995

246 On average, 1.5 medicanes are observed annually in the Mediterranean (Cavicchia et al., 2014;
247 Nastos et al., 2018; Romero and Emanuel, 2013; Zhang et al., 2021) and, more rarely, similar
248 storms are observed over the Black Sea (Yarovaya et al., 2008). We begin with a system,

249 Medicane Celeno, that reached maturity on 16 January, 1995, shown in infrared satellite
250 imagery in Figure 2.
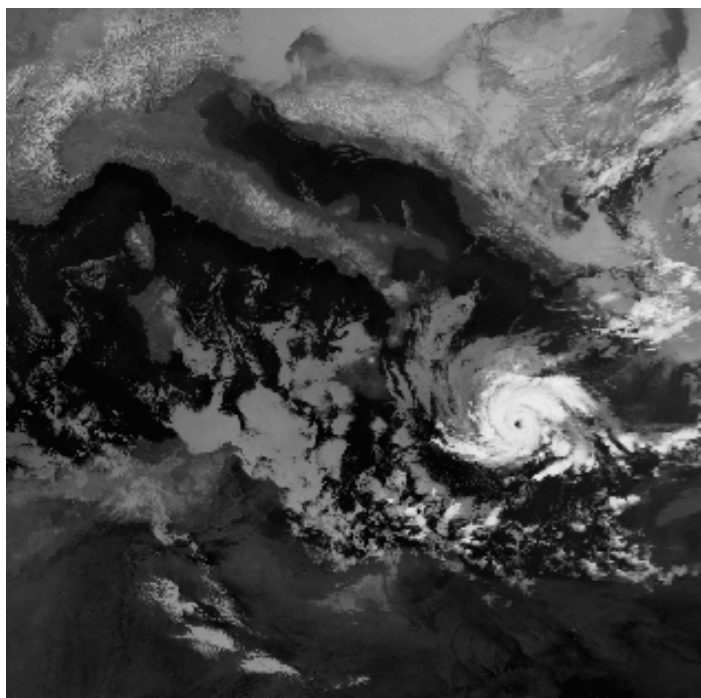
251

252 *Figure 2: Infrared satellite image of Medicane Celeno in the central Mediterranean, at 09:06 UTC 16 January 1995.*
253 *(Image credit: NOAA, 1995)*

254
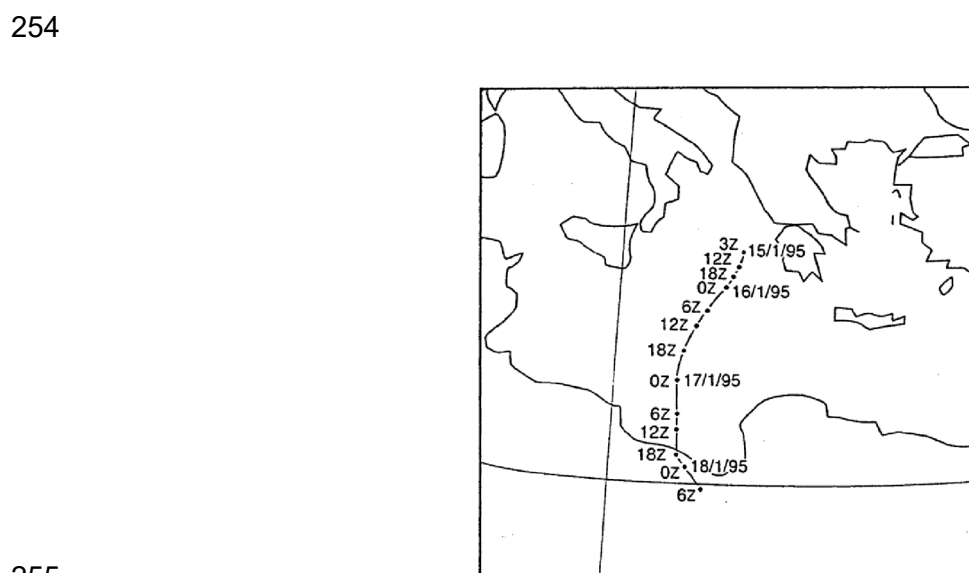
255

256 *Figure 3: Track of the surface center of the cyclone between 03:00 UTC on January 15 and 06:00 on January 18,*
257 *1995, derived from satellite images (Pytharoulis et al.,1999)*

258   Figure 3 shows the track of the surface center of the cyclone, which developed between Greece
259   and Sicily and made landfall in Libya. A detailed description of this medicane is provided by
260   Pytharoulis et al. (1999).

261   The evolution of the system in increments of 24 hours, beginning on 00 ~~GMT~~UTC, 12 January
262   and ending at 00 ~~GMT~~UTC 15 January, is shown in Figure 4. This sequence, showing the 400
263   hPa and 950 hPa geopotential heights, covers the period ~~just before the system~~
264   ~~develops~~leading up to the cyclop development. The evolution of the upper tropospheric (400
265   hPa) height field shows a classic Rossby wave breaking event (McIntyre and Palmer, 1983) in
266   which an eastward-moving baroclinic Rossby wave at higher latitudes amplifies and irreversibly
267   breaks to the south and west, finally forming a cut-off cyclone. It is important to note that the
268   formation of a cutoff cyclone in the upper troposphere involves a local conversion of kinetic to
269   potential energy, with deep cooling associated with dynamically forced ascent. To the southeast
270   of this trough, a weak, broad area of low ~~pressure~~ geopotential height develops at 950 hPa
271   mostly over land in a region of low-level warm advection. As the cold ~~pool~~ air under the cut-off
272   low is gradually heated by the underlying sea, a broad surface cyclone develops by 00
273   ~~GMT~~UTC on January 14th. At around this time, the feedback between surface wind and surface
274   enthalpy fluxes is strong enough to develop a tight inner warm core (warm, that is, relative to the
275   surrounding cold pool, not necessarily to the unperturbed larger scale environment) and by 00
276   ~~GMT~~UTC on January 15th, it is noticeable just to the west of northwestern Greece (Figure 5d).
277   At the same time, the upper cold core weakens, perhaps ~~no doubt~~ aided by the strong heating
278   from the surface transferred aloft by deep convection.

279
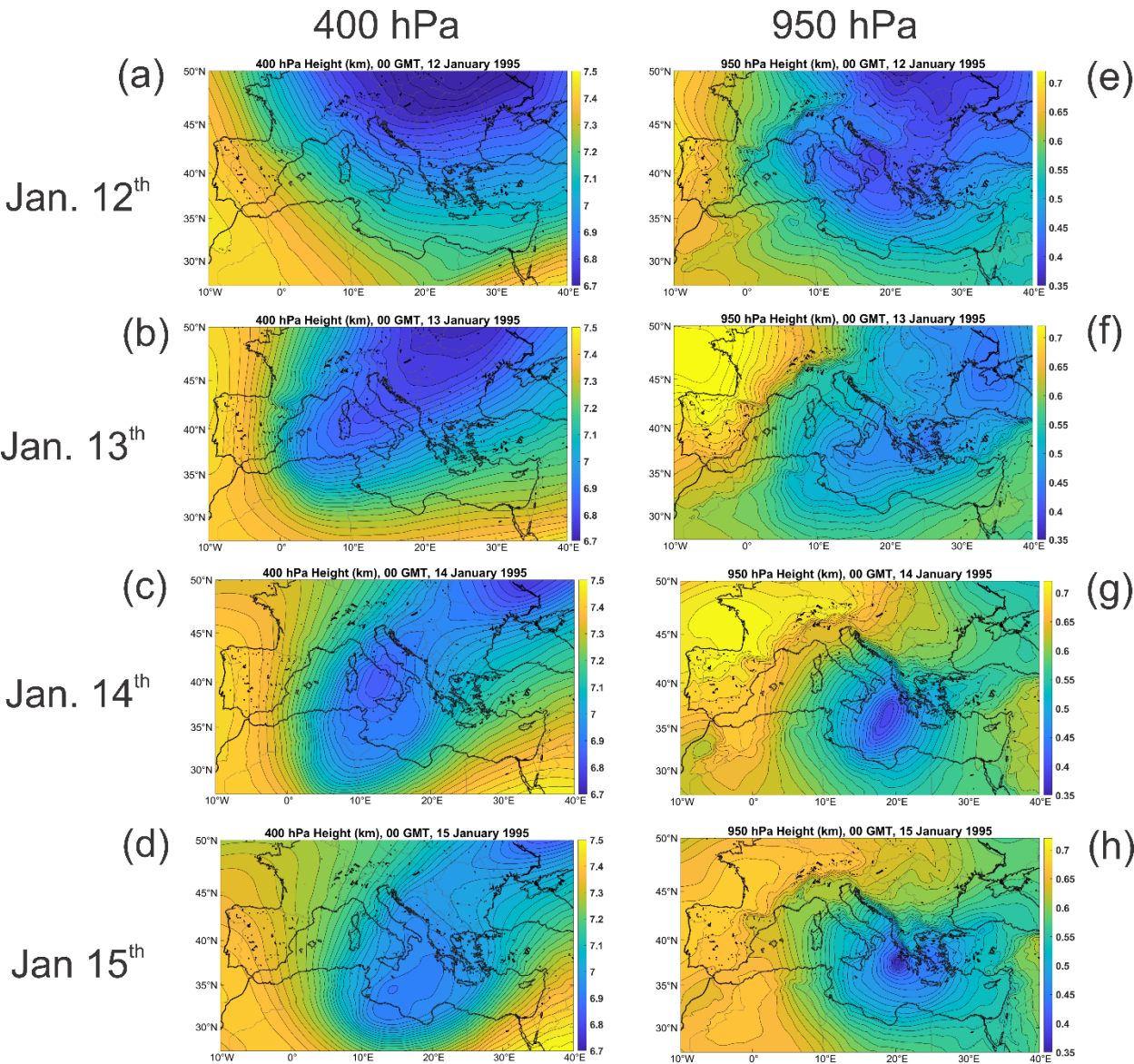
Figure 4: Evolution of the 400 hPa (left) and 950 hPa (right) geopotential heights in 24-hour increments, from 00 ~~GMT~~UTC 12 January to 00 ~~GMT~~UTC 15 January, 1995. These fields are from ERA5 reanalysis. The 400 hPa heights span from 6.7 to 7.5 km at increments of 26.67 m, while the 950 hPa heights range from 350 m to 730 m at increments of 12.67 m.

280

281
282
283
284
285

750 hPa T (K)   Modified Potential Intensity (m/s)

286
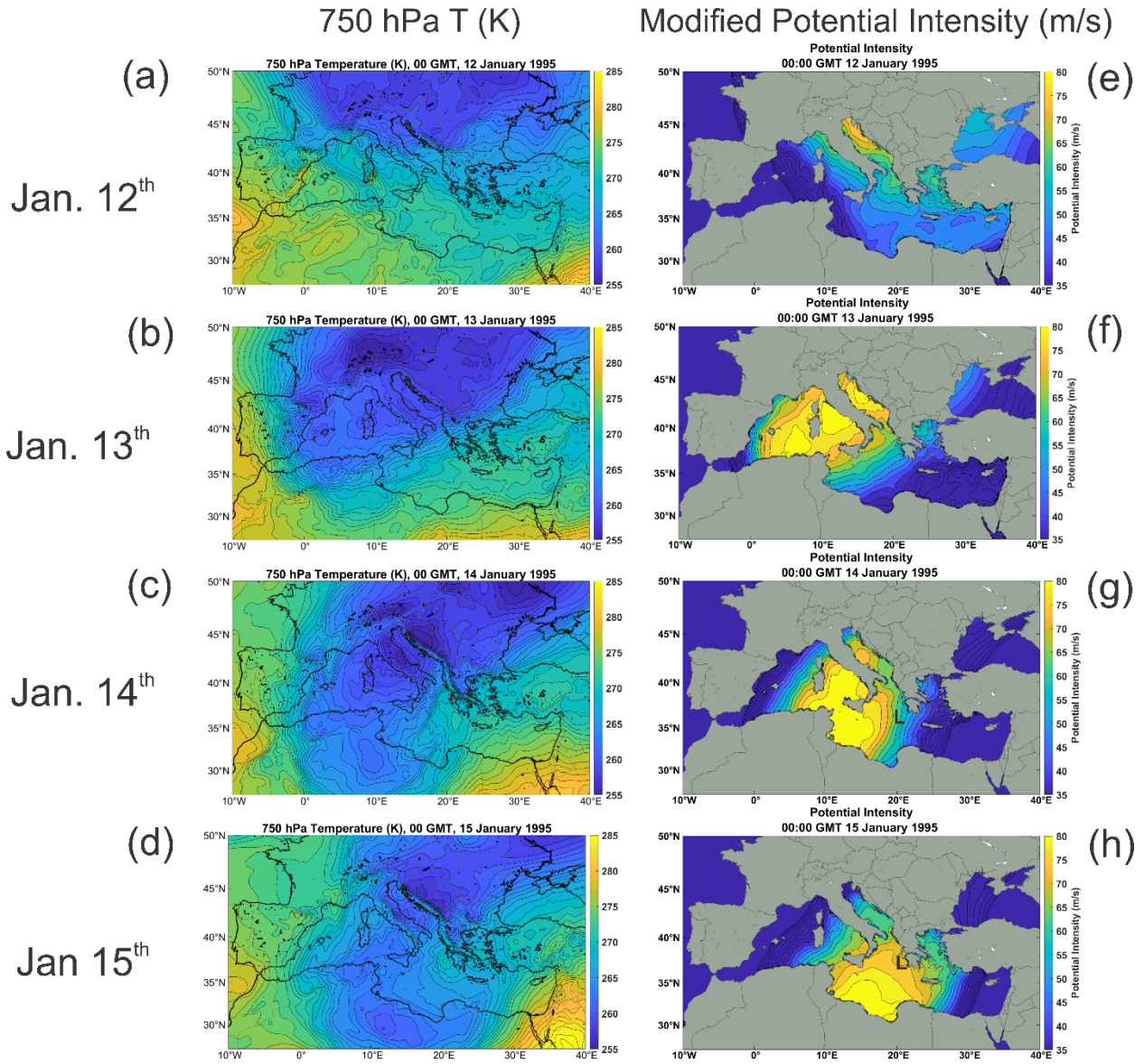
Figure 5: 750 hPa temperature (K; left) and modified potential intensity given by equation (1) (m/s, right) at 00
~~GMT~~UTC on January 12th – 15th (top to bottom) 1995. The 750 hPa temperature spans from 255 K to 285 K at
increments of 1 K, while the modified potential intensity ranges from 35 to 80 ms⁻¹ ~~.~~ at increments of 4 ms⁻¹. The black
"Ls" in panels g) and h) show the positions of the surface cyclone. From ERA5 reanalysis.

291

292

Figure 5 shows the corresponding evolution of the 750 hPa temperature and the modified

potential intensity, V_{pm}, given by (1). The latter in this and subsequent figures is only shown in

295   the range of $35\,ms^{-1}$ to $80\,ms^{-1}$. Experience shows that tropical cyclone genesis is rare when

296   the potential intensity is less than about $35\,ms^{-1}$ (Emanuel, 2010).

297   On January 12th, relatively small values of V_{pm} are evident in the eastern and northern

298   Mediterranean, but with higher values developing over the northern Adriatic as cold air aloft

299   creeps in from the north. As the upper tropospheric Rossby wave breaks and a cut-off cyclone

300   develops over the central Mediterranean, V_{pm} increases greatly during the 13th and 14th, with

301   peak values greater than $80\,ms^{-1}$. The cyclop develops in a region of very high V_{pm}, though not

302   where the highest values occur. Note that a lower warm core is not obvious at 750 hPa until

303   January 15th and that it occurs on a somewhat smaller scale than the cut-off cyclone.

304   As the cyclop moves southward, it maintains a tight inner warm core until after landfall (not

305   shown here) and the modified potential intensity, V_{pm}, over the south-central Mediterranean

306   diminishes rapidly, with peak values of only about $60\,ms^{-1}$ by 00 ~~GMT~~UTC on January 17th.

307   One potentially important difference between cyclop development and tropical transition is that

308   in the former case, the volume of air with appreciable potential intensity is limited. It is possible

309   that, by warming the whole tropospheric column relative to the surface, the enhanced surface

310   fluxes associated with the cyclop, acting through deep convection, substantially diminish the

311   magnitude and/or volume of the high V_{pm} air, serving to limit the lifetime of the cyclop. This was

312   the case in the axisymmetric numerical simulations of Emanuel (2005).

313   It is clear ~~in this case~~ that this cyclop development occurred on time and space scales

314   appreciably smaller than those of the rather weak, synoptic-scale cyclogenesis resulting from

315   the interaction of the positive PV perturbation near the tropopause with a low-level temperature

316   gradient. It is also clear that the strong cooling of the troposphere in response to the

317   development and southward migration of the cutoff cyclone aloft was instrumental in bringing

318   about the high potential intensity necessary to activate the WISHE process. Therefore, the

319   Rossby wave breaking did much more than trigger cyclogenesis; it provided the necessary

320   potential intensity for the cyclop development. Here we draw a distinction from tropical

321   transition, in which, in most cases, the pre-existing potential intensity suffices to maintain a

322   surface flux-driven cyclone. We emphasize again that there is a gray area here consisting of

323   flux-driven cyclones in which the existing reservoir of potential intensity is enhanced to some

324   degree by the local synoptic-scale dynamics.

325   3.2 Medicane of December 2005

326   A medicane, unofficially known as Zeo, formed on December 14th 2005 off the coast of Tunisia

327   and then moved eastward across a large stretch of the Mediterranean. Figure 6 shows a

328   satellite image of this medicane on December 15th. This cyclone has been the subject of

329   several intensive studies (e.g. Fita and Flaounas, 2018; Miglietta and Rotunno, 2019).

330
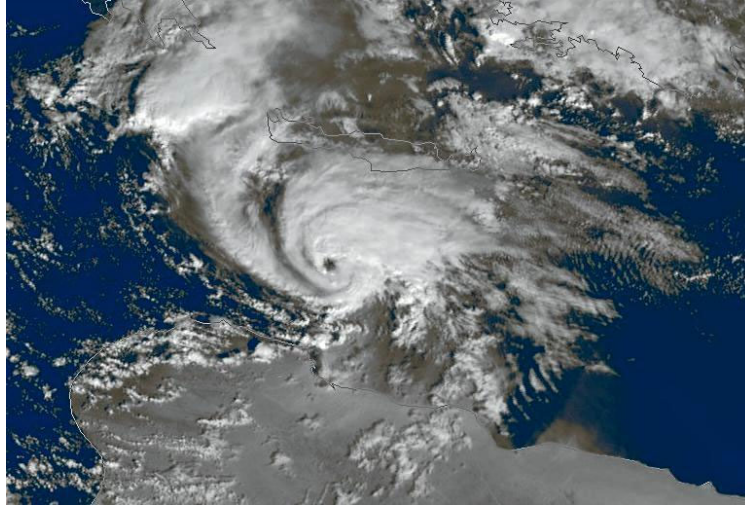
Figure 6: Medicane Zeo between Crete and Libya on 15 December 2005. Image from NASA.

331

332 Like Medicane Celeno, Medicane Zeo formed as a result of a Rossby wave breaking event, as
333 illustrated in Figure 7. On December 8th (panel a), a deep trough is digging southward over
334 eastern Europe, but by the 9th (panel b) it has split in two, with the westward half breaking
335 southwestward over Germany and Switzerland. By the 11th (panel d), this local minimum is
336 located over Tunisia and on the 12th (panel e) it is more or less completely cut off from the main
337 westerly jet. It subsequently oscillates over Tunisia and Algeria, before moving slowly eastward
338 over the Mediterranean, as shown in Figure 8.

339 In response to the cutoff cyclone development, a broad, synoptic-scale surface cyclone formed
340 to the east of the upper cyclone over the deserts of Libya during December 12th and 13th (not
341 shown here). The poorly defined center of this system drifted northward, on collision course with
342 the upper cyclone, which was drifting eastward over Tunisia by late on the 13th. As the surface
343 center moved out over the Mediterranean early on the 13th, rapid development ensued and a
344 mature cyclop was evident by 00 ~~GMT~~UTC on the 14th (Figure 8c). The system began to move
345 eastward and reached peak intensity on the 14th (lower panels of Figure 8). The cyclop moved
346 eastward, along with its parent upper cyclone, and dissipated in the far eastern Mediterranean
347 on the 16th (not shown).

348

349

350
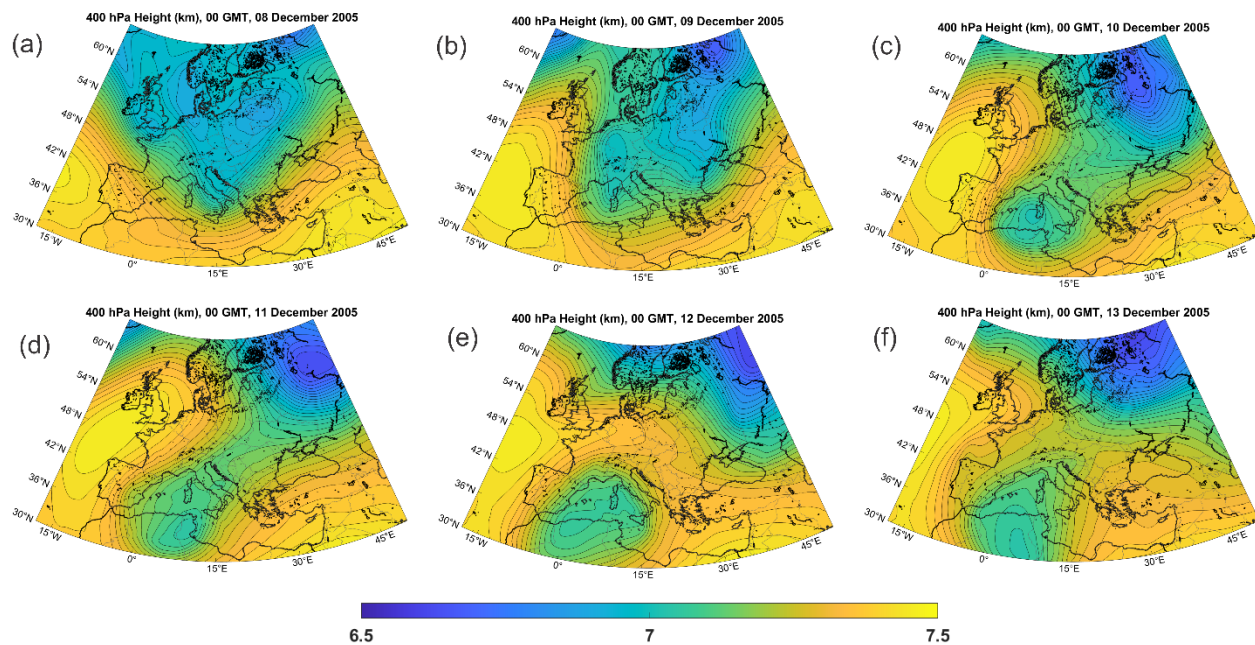
Figure 7: 400 hPa geopotential heights, ranging from 6.5 km to 7.5 km (color scale identical for all panels) at 00
351
~~GMT~~UTC on December 8th (a), 9th (b), 10th (c), 11th (d), 12th (e), and 13th (f), 2005. From ERA-5 reanalysis. Contour
352
interval is 33.3 m.
353

354   The evolutions of 750 hPa temperature and V_{pm} on the 14th and 15th of December are shown in

355   Figure 9. In this case, there were large meridional gradients of sea surface temperature across

356   the Mediterranean, ranging from over 20°C in the far south to less than 12°C in the northern

357   reaches of the Adriatic and western Mediterranean (not shown here). As the cold pool moved

358   southwestward and deepened, only low values of V_{pm} are present over the northern

359   Mediterranean, but beginning on December 10th, higher values developed over the Gulf of

360   Sidra, east of Tunisia, and by the 14th (Figure 9c) had reached at least 80 ms⁻¹, enabling the

361   formation of the cyclop. As in the Celeno case, V_{pm} ~~values diminish t~~ values diminish

362   thereafter, possibly because of the warming of the column by the surface enthalpy flux.

363

364
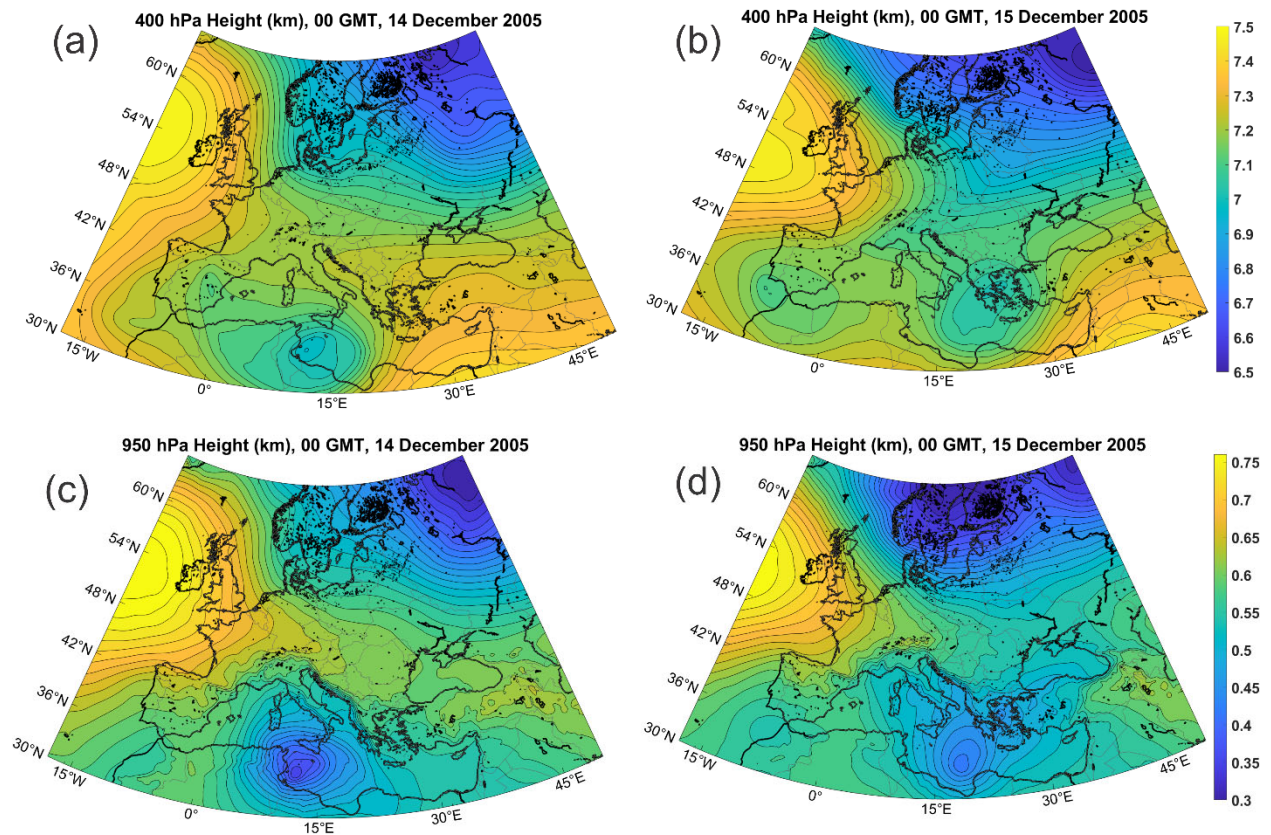
Figure 8: Evolution of 400 hPa geopotential height, ranging from 6.5 to 7.5 km ~~at contour interval of 3~~6.7 m (a and b), and 950 hPa geopotential height, ranging from 250 to 750 m at contour interval of 16.67 m (c and d) at 00 ~~GMT~~UTC in December 14th (left) and 15th (right), 2005. The color scales of (a) and (b) are identical, as are the color scales of (c) and (d). From ERA-5 reanalysis.

369

370

371

372
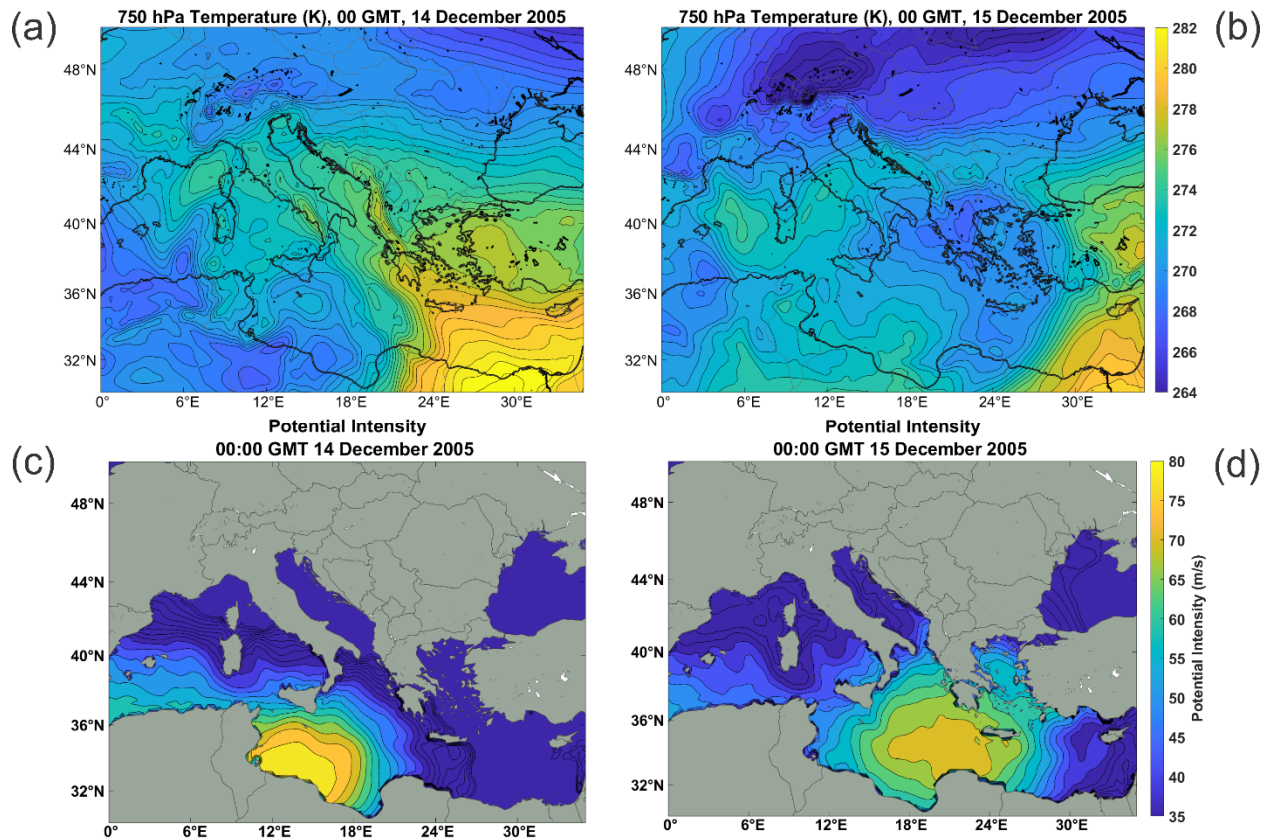
Figure 9: 750 hPa temperature at increments of 0.6 K (a-b) and modified potential intensity at increments of 4 m s⁻¹ (c-d) at 00 ~~GMT~~UTC on December 14th (a,c) and December 15th (b,d) 2005. From ERA-5 reanalysis.

373
374

The 750 hPa temperature field (Figure 9a) shows a complex pattern of positive temperature perturbation near the position of the surface low, not nearly as focused as in the case of medicane Celeno. As suggested by Fita and Flaounas (2018), part of the positive temperature anomaly associated with the cyclone may have resulted from a warm seclusion. Yet 24 hours later (Figure 9b) the warm anomaly near the cyclone center over the eastern Gulf of Sidra appears to have been advected from the south rather than the north. It is possible that the reanalysis did not capture the full physics of this particular medicane.

Figure 10 compares total column water retrieved from satellite microwave and near-infrared imagers (a) to that from the ERA5 reanalysis (b). While there is some broad agreement between the two estimates, the ERA5 underestimates column water in the critical region just east of Tunisia and overestimates it in an arc extending from eastern Sicily southeastward to the Libyan coast. Cyclop intensity, in analogy to tropical cyclone intensity, should be highly sensitive to low- and mid-level moisture in the mesoscale inner core region, which ~~and~~ may be under-resolved and otherwise not well simulated by global NWP models. For this reason, we do not routinely show reanalysis of water vapor in this paper. The limitations of analyzed and forecast water vapor may constitute an important constraint on cyclop predictability and is a worthy subject for future research.

392
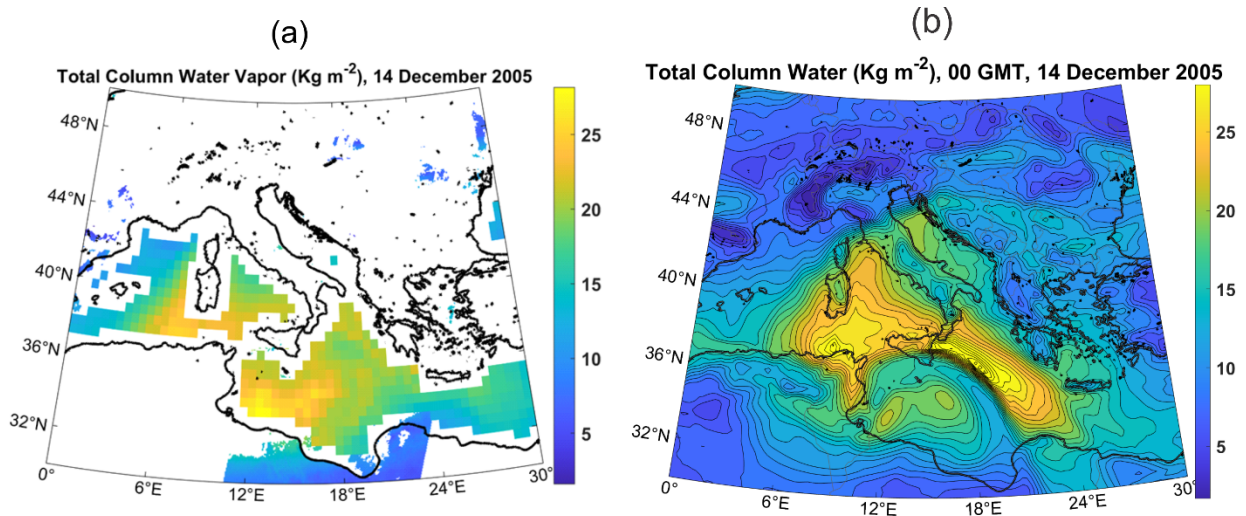
Figure 10: Total column water vapor (Kg m⁻²) at 00 ~~GMT~~UTC on 14 December 2005, derived from microwave and
near infrared imagers (a) and ERA5 reanalysis (b). In (b) the contour increment is 0.9 Kg m⁻².

395

3.3 Polar low of February, 1987

Closed upper tropospheric lows also provide favorable environments for cyclop development at
very high latitudes in locations where there is open water. These usually form poleward of the
mid-latitude jet, where quasi-balanced dynamics can be quite different from those operating at
lower latitudes. Figure 11 is an infrared image of a polar low that formed just south of Svalbard
on February 25th, 1987, and tracked southward, making landfall on the north coast of Norway on
the 27th. This system was studied extensively by Nordeng and Rasmussen(1992).

403
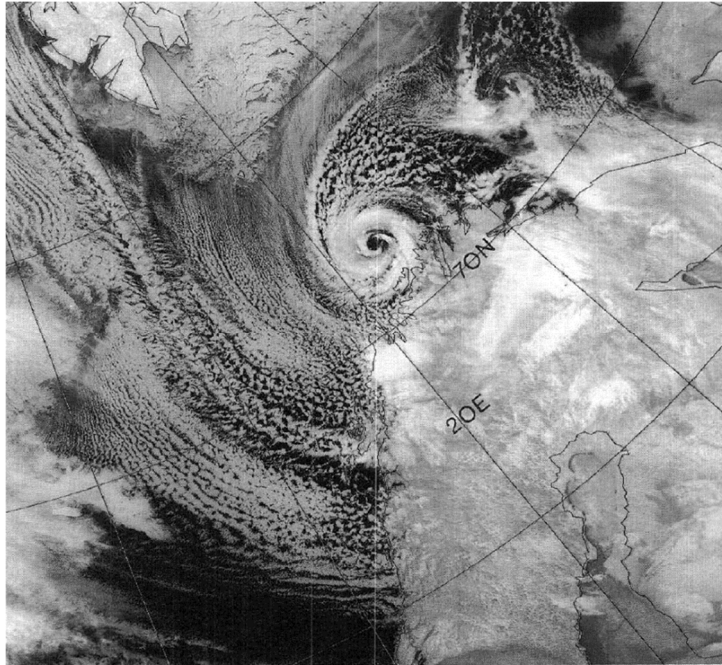
Figure 11: NOAA 9 satellite infrared image (channel 4) of a polar low just north of Norway at 08:31 ~~GMT~~UTC on 27 February 1987.

As with some medicanes, polar lows develop in strongly convecting air masses when cold air moves out over relatively warm water. The adjective "relatively" is crucial here; with polar lows the sea surface temperature is often only marginally above the freezing point of saltwater. Figure 12 shows the distribution of sea surface temperature on February 25th, with the uniform dark blue areas denoting regions of sea ice cover. The polar low shown in Figure 11 develops when deep cold air moves southward over open water, as shown in Figure 13.

In this case, it is not clear whether one can describe what happens in the upper troposphere (top row of Figure 13) as a Rossby wave breaking event. Instead, what we see is a complex rearrangement of the tropospheric winter polar vortex, as a ridge building over North America breaks and forms an anticyclone over the North Pole. This complex rearrangement results in the formation of a deep cutoff low just south of Svalbard by the 26th, which then moves southward over Norway by the 27th. The polar low is barely visible in the 950 hPa height field on the 25th (middle row of Figure 13), but intensifies rapidly as it moves over progressively warmer water, reaching maturity before landfall on the 27th.

420

421
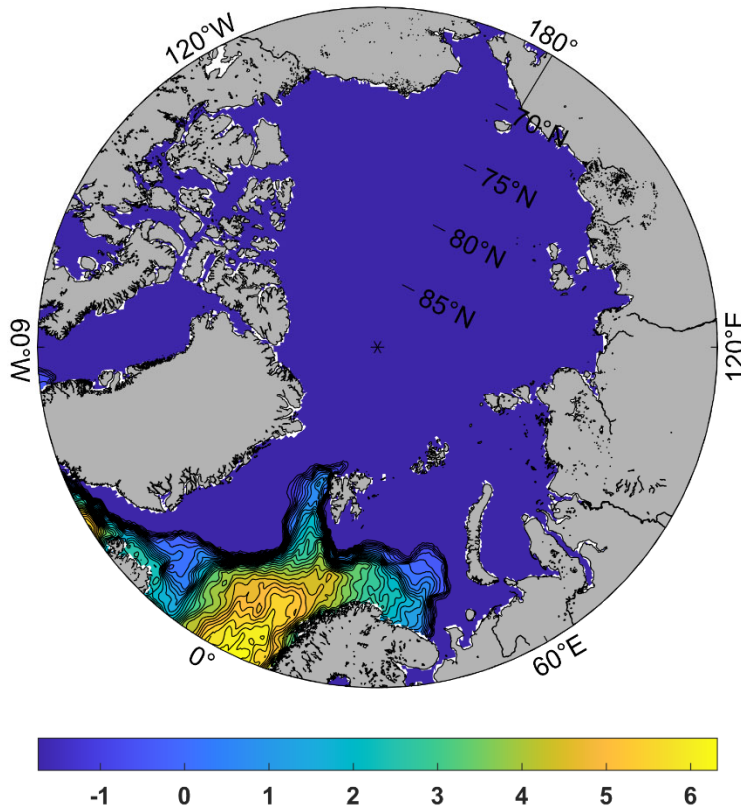
Figure 12: Sea surface temperature (ºC) in intervals of 0.3ºCat 02:00 ~~GMT~~UTC on 25 February, 1987, from ERA5 reanalysis. Dark blue areas denote regions of sea ice. From ERA-5 reanalyses.

422
423

424   The evolution of the V_{pm} field is shown in the bottom row of Figure 13. The potential intensity

425 increases rapidly south of Svalbard as the cut-off cyclone moves out over open water. (The

426 secondary region of high potential intensity, poleward of Siberia, is owing to relatively high ice

427 surface temperature in a region covered with sea ice. As there is very little heat flux through sea

428 ice, a cyclop cannot develop in this region, but a weak and broad surface low is associated with

429 the cutoff cyclone in the upper troposphere.)

430   Under these conditions, ~~almost all~~ most of the surface flux that drives the cyclop is in the form of

431 sensible, rather than latent heat flux, and the background state has a nearly dry (rather than

432 moist) adiabatic lapse rate. As shown by Cronin and Chavas (2019) and Velez-Pardo and

433 Cronin (2023), surface flux-driven cyclones can develop in perfectly dry convecting

434 environments, though they generally reach smaller fractions of their potential intensity and lack

435 the long tail of the radial profile of azimuthal winds that is a consequence of the dry stratification

436 resulting from background moist convection (Chavas and Emanuel, 2014). They also have

437 larger eyes relative to their overall diameters. Given the low temperatures at which they occur,

438 polar lows may be as close to the Cronin-Chavas dry limit as one might expect to see in Earth's

439 climate.

440
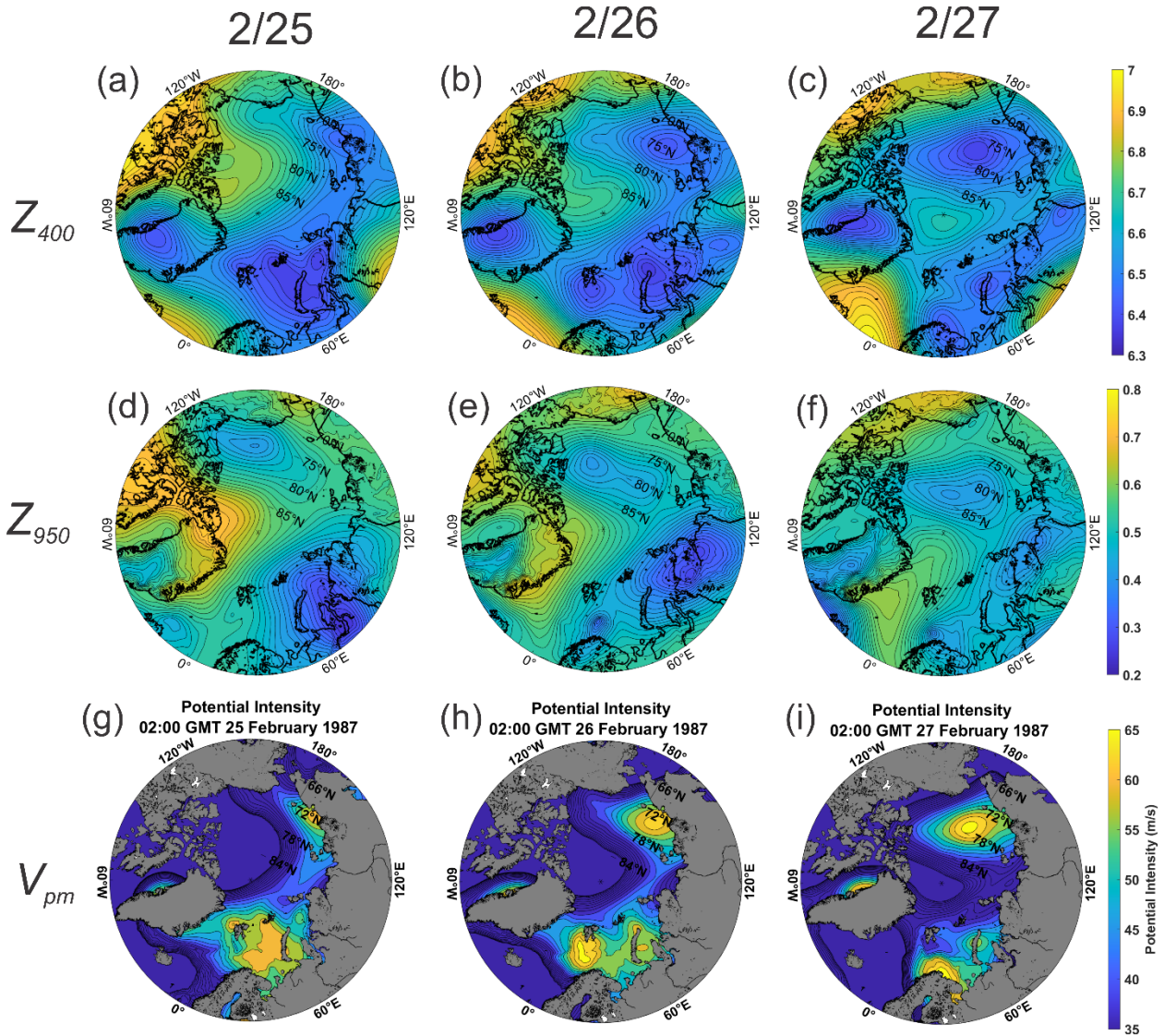
Figure 13: 400 hPa geopotential height (km)t at intervals of 23.3 m (a-c), 950 hPa geopotential height (km) in
441

442 *intervals of 20 m (d-f), and V_{pm} (ms⁻¹) in intervals of 3.25 ms⁻¹ (g-i), at 02:00 ~~GMT~~UTC on February 25th (left), 26th*

443 *(center), and 27th (right), 1987. From ERA-5 reanalysis.*

444 One interesting feature of polar waters in winter is that the thermal stratification is sometimes
445 reversed from normal, with warmer waters lying beneath cold surface waters. This is made
446 possible, in part, by strong salinity stratification, that keeps the cold water from mixing with the
447 warmer waters below. Therefore, it is possible for polar lows to generate warm, rather than cold,
448 wakes, and this would feed back positively on their intensity. This seems to happen in roughly
449 half the documented cases of polar lows in the Nordic seas (Tomita and Tanaka, 2024).

3.4 Polar low over the Sea of Japan, December, 2009

Polar lows are not uncommon in the Sea of Japan, forming when deep, cold air masses from Eurasia flow out over the relatively warm ocean. They are frequent enough to warrant a climatology (Yanase and co-authors, 2016). A satellite image of one such storm is shown in Figure 14.
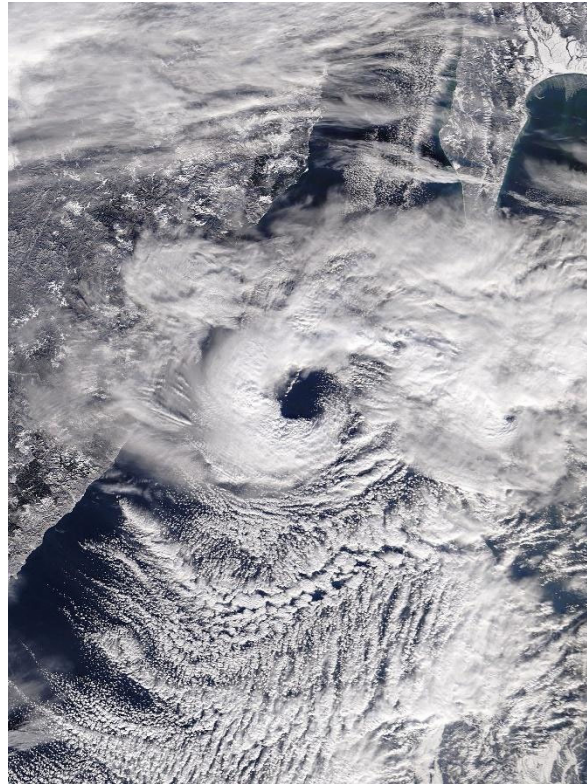
Figure 14: Polar low over the northern Sea of Japan, 02:13 ~~GMT~~UTC 20 December, 2009 as captured by the MODIS imager on NASA's Terra satellite.

The cyclone traveled almost due south from this point, striking the Hokkaido region of Japan, near Sapporo, with gale-force winds and heavy snow. As with other cyclops, it formed in an environment of deep convection under a cold low aloft.

The development of the cutoff cyclone aloft was complex, as shown by the sequence of 400 hPa maps displayed in Figure 15. These are 00 ~~GMT~~UTC charts at 1-day intervals beginning on December 11th and ending on the 20th, about the time of the image in Figure 14. A large polar vortex is centered in northern central Russia on the 11th but sheds a child low southeastward on the 12th and 13th, becoming almost completely cutoff on the 14th. The parent low drifts westward during this time. The newly formed cutoff cyclone meanders around in isolation from the 15th through the 17th, but becomes wrapped up with a system propagating into the domain from the east on the 18th. By the 20th, a small-scale cutoff cyclone is drifting southward over the northern Sea of Japan, and it is this upper cutoff that spawns the polar low.

470
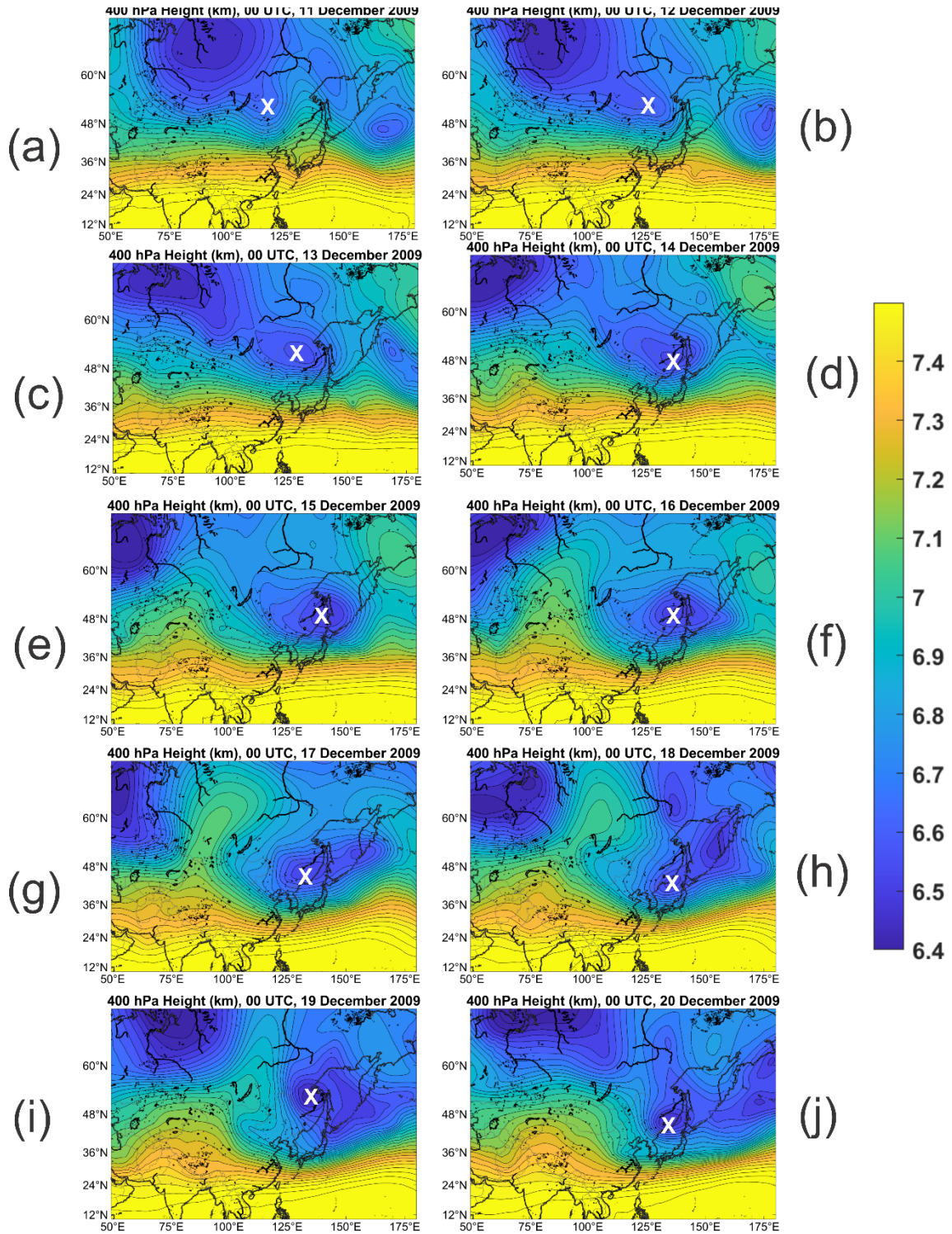
Figure 15: Sequence of 400 hPa geopotential height (km) charts at 1-day intervals from 00 ~~GMT~~UTC on December 11ᵗʰ (a) to 00 ~~GMT~~UTC on December 20ᵗʰ (j), 2009. The charts span from 0º to 180º longitude and from 10º to 70º latitude, and the contour increment is 36.7 m. The white crosses mark the center of the 400 hPa cyclone that was ultimately associated with the polar low. From ERA-5 reanalysis.

475   The 950 hPa height and the V_{pm} fields at 00 ~~GMT~~UTC on December 20th are shown in Figure

476   16. At this time, the surface low is developing rapidly and moving southward into a region of

477   high potential intensity. The latter reaches a maximum near the northwest coast of Japan,

478   where the sea surface temperatures are larger. As with the two medicane cases and the other

479   polar low case, the cyclop develops in a place where the potential intensity values are normally

480   too low for surface flux-driven cyclones but for which the required potential intensity is created

481   by the ~~approach~~ movement of a deep cold cyclone aloft over relatively warm water. The

482   reanalysis 750 hPa temperature (not shown) presents a local maximum at the location of the

483   surface cyclone at this time.

484   (a)   (b)
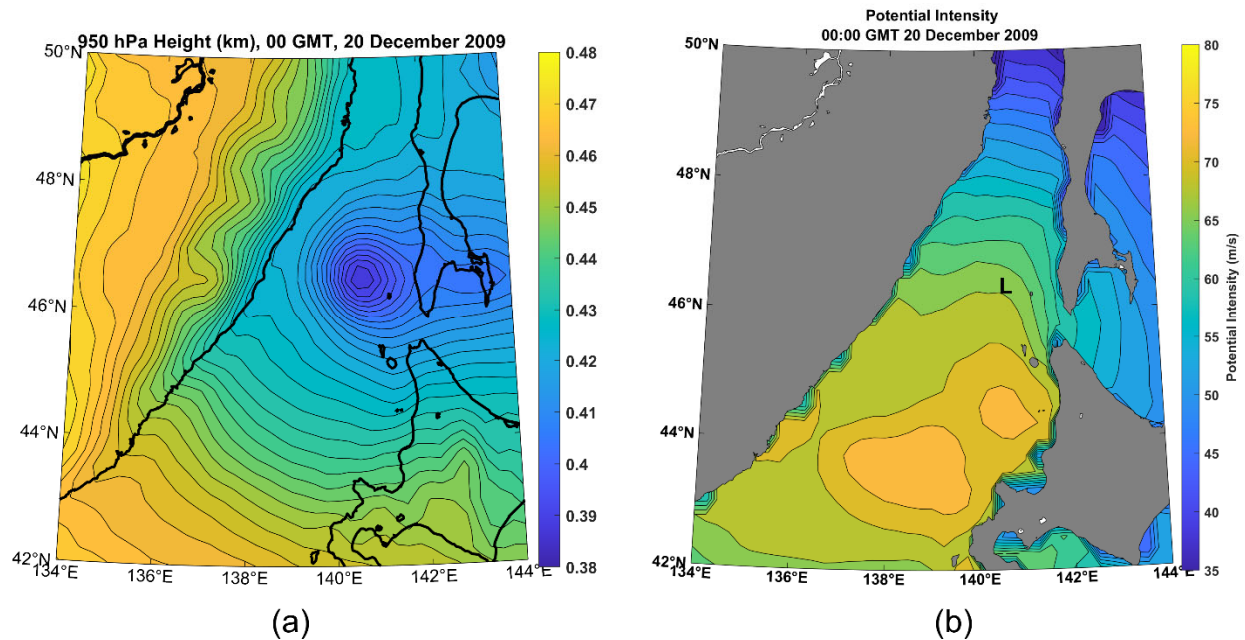
485   *Figure 16: 950 hPa geopotential height (a; km) at intervals of 3 m, and V_{pm} at intervals of 4 m s⁻¹ (b), at 00 ~~GMT~~UTC*

486   *on 20 December, 2009. In (b), the "L" marks the satellite-derived surface cyclone center. From ERA-5 reanalysis.*

487

3.5 The subtropical cyclone of January, 2023

489   The term "subtropical cyclone" has been used to describe a variety of surface flux-assisted

490   cyclonic storms that do not strictly meet the definition of a tropical cyclone. The term has an

491   official definition in the North Atlantic[4] but is used occasionally elsewhere, especially in regions

492   where terms like medicane, polar low, and Kona storm do not apply, such as the South Atlantic

493   (Evans and Braun, 2012; Gozzo et al., 2014). Here we will use the term to designate cyclops in

494   the sub-arctic North Atlantic; that is, surface flux-powered cyclones that develop in regions and

---

[4] The National Hurricane Center defines a "subtropical cyclone" as "a non-frontal low-pressure system
that has characteristics of both tropical and extratropical cyclones", but in the past has also used the
terms "hybrid storm" and "neutercane".

495   times whose climatological thermodynamic potential is small or zero, that would not be called
496   polar lows owing to their latitude. This usage may not be consistent with other definitions. The
497   point here is to show that cyclops can occur in the North Atlantic and we can safely refer to
498   these as cyclops whether or not they meet some definition of "subtropical cyclone".

499   Figure 17 displays a visible satellite image of a subtropical cyclone over the western North
500   Atlantic on 16 January, 2023. It resembles the medicanes and polar lows described previously,
501   and like them, formed under a cutoff cyclone aloft.

502
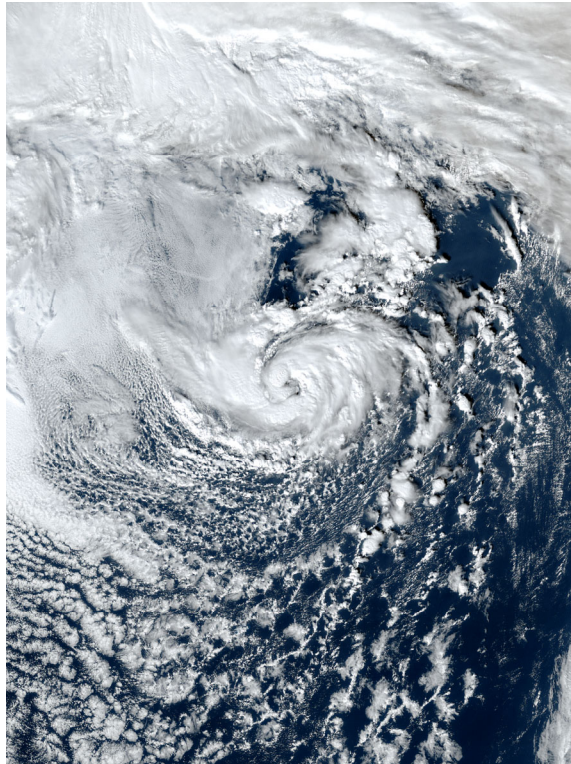
503   *Figure 17: Subtropical cyclone over the western North Atlantic, 18:20 ~~GMT~~UTC, 16 January 2023. NOAA*
504   *geostationary satellite image.*

505   The formation of the cutoff cyclone aloft is shown in Figure 18. A deep trough advances slowly
506   eastward over eastern North America and partially cuts off on the 14th. As the associated cold
507   pool and region of light shear migrate out over the warm waters south of the Gulf Stream, a
508   cyclop forms and intensifies with peak winds of around 60 kts at around 00 ~~GMT~~UTC on the 17th
509   (Cangliosi et al., 2023). Note also the anticyclonic wave breaking event to the east of the
510   surface cyclone development, in the eastern half of panels 18b-d.

511   The evolutions of the 950 hPa and associated V_{pm} fields are displayed in Figure 19. (Note the
512   smaller scale around the developing surface cyclone, compared to Figure 18.) On January 14th,
513   the only appreciably large values of V_{pm} are associated with ~~in~~ the Gulf Stream and in the far
514   southwestern portion of the domain. The 950 hPa height field shows a broad trough associated

515 with the baroclinic wave moving slowly eastward off the U.S. east coast. But as the upper cold

516 cyclone moves out over warmer water on the 15th, large V_{pm} develops south of the Gulf Stream,

517 and a closed and more intense surface cyclone develops under the lowest 400 hPa heights and

518 over the region with higher V_{pm} values.

519

520
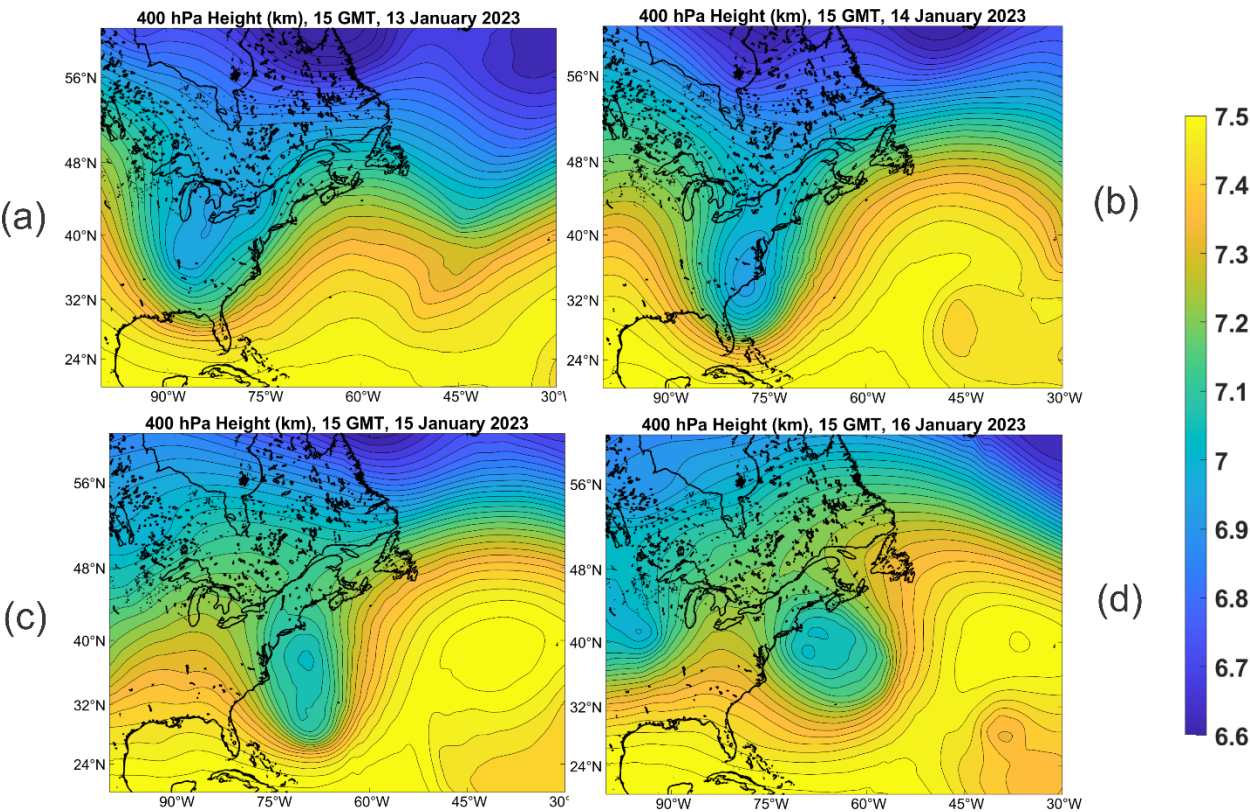
521 *Figure 18: 400 hPa geopotential height (km) at intervals of 30 m, at 15:00 ~~GMT~~UTC on January 13th (a), 14th (b), 15th*
522 *(c), and 16th (d), 2023. From ERA-5 reanalysis.*

523

(a)   (b)   (c)

(d)   (e)   (f)

524
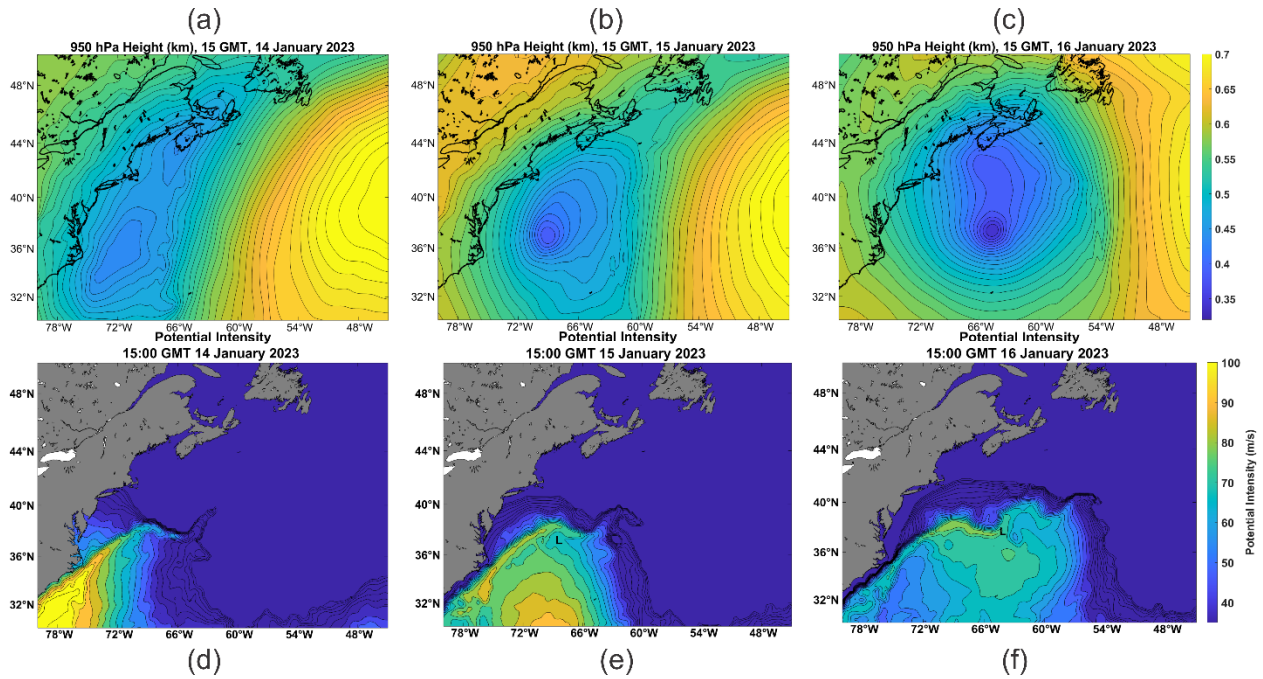
525 *Figure 19: The 950 hPa geopotential height (km) at 15:00 ~~GMT~~ UTC on January 14th (a), 15th (b), 16th (c); the V_{pm}*
526 *field on January 14th (d), 15th (e), and 16th(f). In (e) and (f) the "L" shows the position of the 950 hPa cyclone center at*
527 *the time of the chart. From ERA-5 reanalysis.*

528 As the upper tropospheric cyclone begins to pull out toward the northeast on the 16th, the
529 surface cyclone intensifies in the region of large V_{pm} south of the Gulf Stream, while the more
530 gradual warming of the surface air in the region of small V_{pm} north of the Stream yields surface
531 pressure falls, but not as concentrated and intense as in the cyclop to the south.

532 Although the evolution of the upper tropospheric cyclone differs in detail from the previously
533 examined cases, and the sharp gradient of sea surface temperature across the north wall of the
534 Gulfstream clearly plays a role here, in other respects the development of this subtropical
535 cyclone resembles that of other cyclops, developing in regions of substantial thermodynamic
536 potential that result, at least in part, from cooling aloft on synoptic time and space scales.

537   3.6 A Kona Storm

538 Hawaiians use the term "Kona Storm" to describe cold-season storms that typically form west of
539 Hawaii and often bring damaging winds and heavy rain to the islands. The term "Kona"
540 translates to "leeward", which in this region means the west side of the islands. They may have
541 been first described in the scientific literature by Daingerfield (1921). Simpson (1952) states that
542 Kona Storms possess "cold-core characteristics, with winds and rainfall amounts increasing with
543 distance from the low-pressure center and reaching a maxima at a radius of 200 to 500 mi.
544 However, with intensification, this cyclone may develop warm-core properties, with rainfall and

545 wind profiles bearing a marked resemblance to those of the tropical cyclone." In general,
546 Simpson's descriptions of the later stages of some Kona Storms are consistent with them being
547 cyclops. But it should be noted that the term is routinely applied to cold-season storms that
548 bring hazardous conditions to Hawaii regardless of whether they have developed warm cores. A
549 good review of the climatology of Kona storms is provided by Otkin and Martin (2004), who state
550 that "development of the surface cyclone in all types results from the intrusion of an upper-level
551 disturbance of extratropical origin into the subtropics". Here we focus on ~~those that do~~ Kona
552 storms that do develop warm cores, providing as a first ~~single~~ example the Kona Storm of 19
553 December 2010. A visible satellite image of this storm is shown in Figure 20.

554
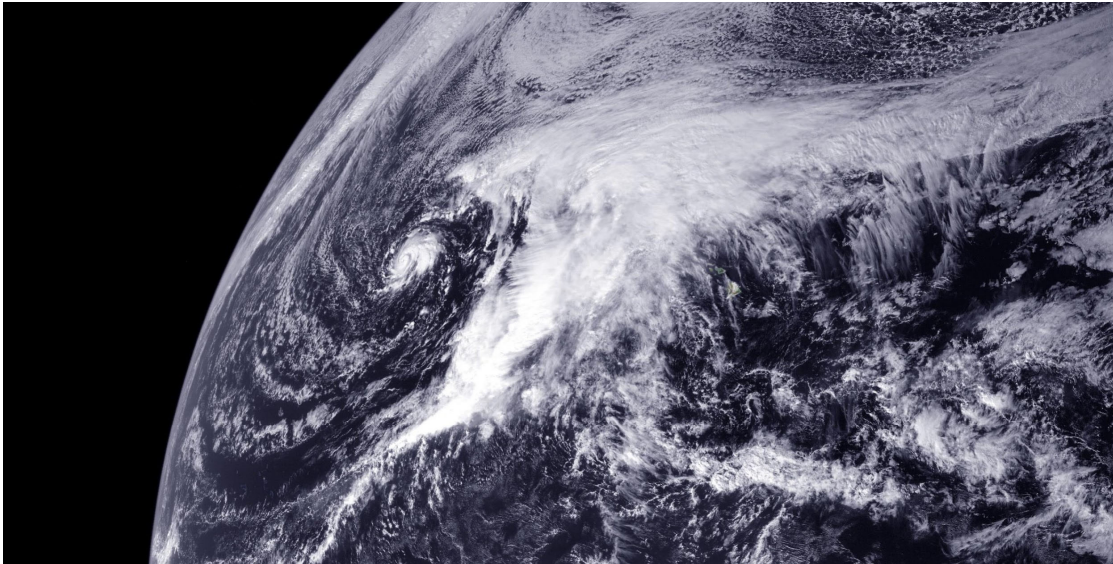
555 *Figure 20: Geostationary satellite visible image showing a Kona Storm at 00 ~~GMT~~UTC on 19 December 2010. The*
556 *Kona Storm is the small-scale cyclone left of the major cloud mass. (Image credit: NOAA-NASA GOES Project,*
557 *2010.)*

558
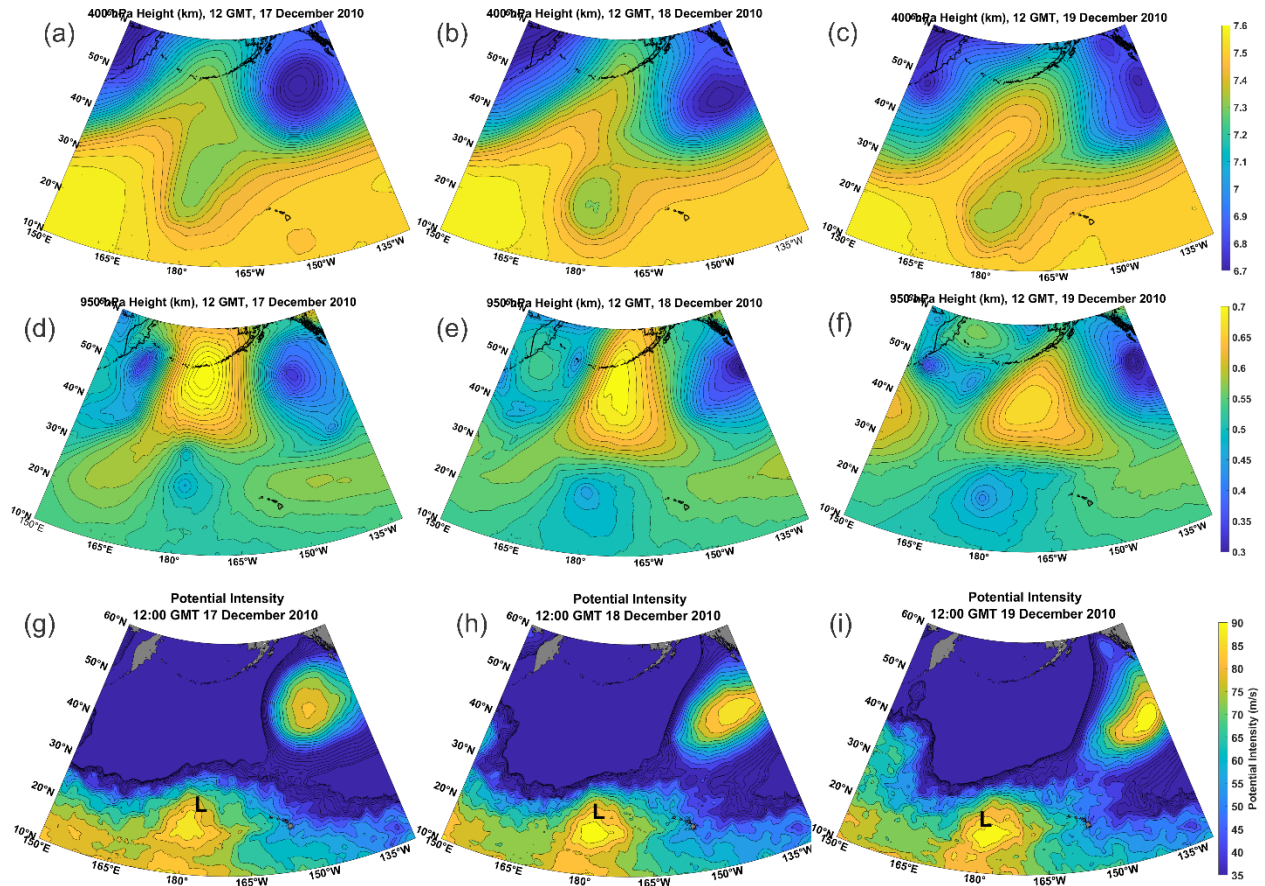
Figure 21: Sequence of 400 hPa geopotential height charts (km) at contour intervals of 30 m (a)-(c)), 950 hPa
geopotential heights (km) with contour intervals of 13.34 m (d)-(f)), and V_{pm} with contour intervals of 4.5 ms-1 ((g)-(i))
at 12:00 ~~GMT~~UTC on December 17th ((a), (d), (g)), December 18th ((b), (e), (h), and December 19th ((c), (f), (i)) 2010.
The "L"s in ((g)-(i)) denote the positions of the 950 hPa cyclone center. From ERA-5 reanalysis.

As with all known cyclops, the December 2010 Kona Storm developed under a cold-core cutoff
cyclone aloft, as shown in Figure 21. The upper-level cyclone had a long and illustrious history
before December 18th, having meandered over a large swath of the central North Pacific. But
beginning on December 17th, the cutoff cyclone made a decisive swing southward over waters
with higher values of V_{pm}. A broad surface cyclone was present underneath the cold pool aloft

on all three days, but developed a tight inner core on the 19th as the cold pool slowly drifted over
a region of higher potential intensity.

This Kona Storm developed in a region of modest climatological potential intensity that was,
however, substantially enhanced by the cutoff cyclone aloft. For example, on December 17th,
the conventional (unmodified) potential intensity at the position of the 950 hPa cyclone center
was about 55 ms^{-1}, compared to the 75-80 ms^{-1} values of the modified potential intensity. One
can only speculate whether a surface flux-driven cyclone would have developed without the
enhanced cooling associated with the cutoff cyclone aloft.

576   The Kona Storm of March, 1951 is a more unambiguous case of a cyclop. Figure 22 shows the
577   950 hPa geopotential height field of another Kona Storm, that of March, 1951. The storm, at that
578   time, was classified by the Joint Typhoon Warning Center as a tropical cyclone, but the
579   climatological potential intensity there at that time of year could not have supported any tropical
580   cyclone. Figure 22c shows that substantial V_{pm} was associated with a cutoff cyclone in the upper
581   troposphere, making possible the existence of thisa cyclop.

582
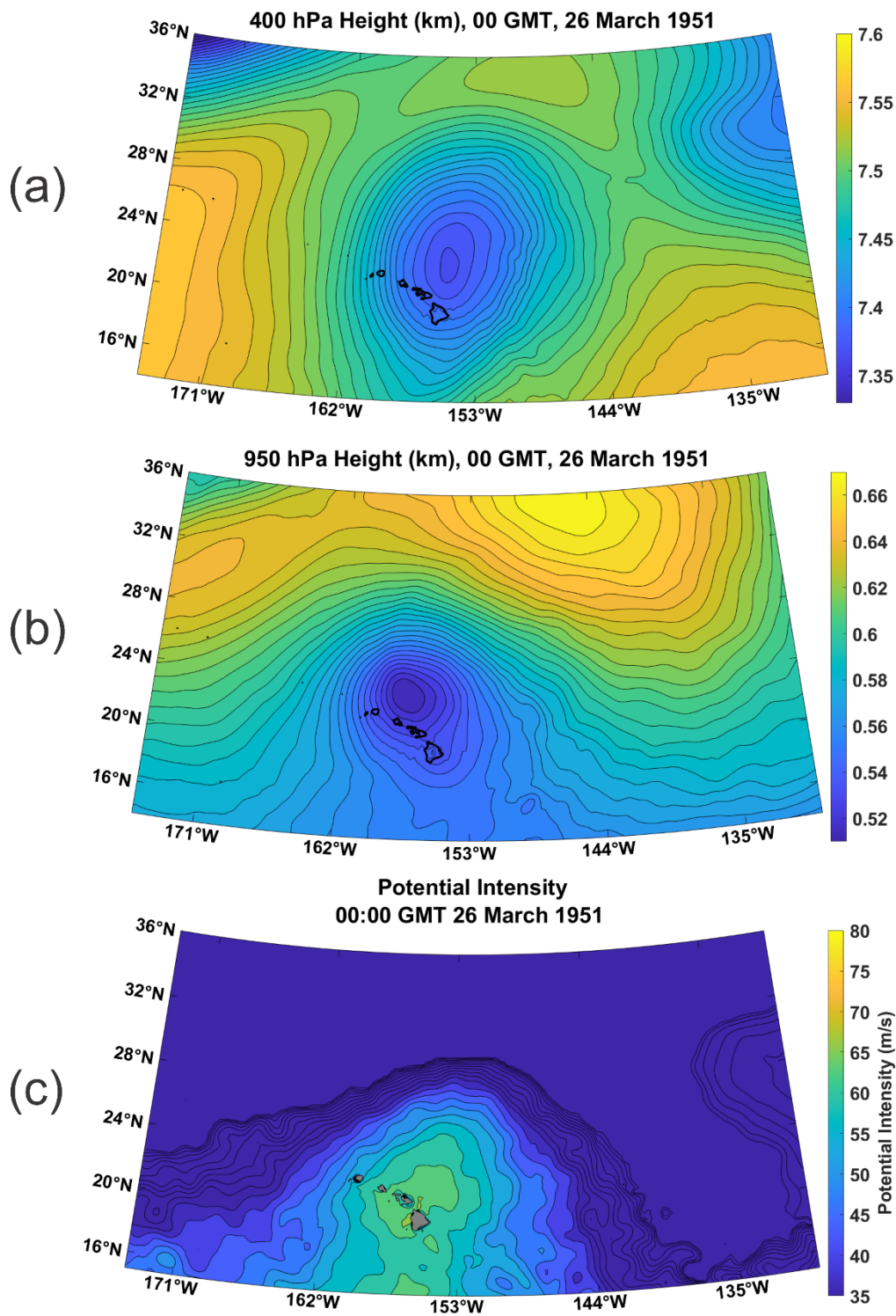
Figure 22: Kona Cyclone of March, 1951. Fields are shown at 00 ~~GMT~~UTC on 26 March: a): 400 hPa geopotential height (km)with a 10 m contour interval, b): 950 hPa geopotential height (km) with 5m contour interval, and c): V_{pm} with a contour interval of 4 ms^{-1}.

583
584
585

4. Variations on the Theme

We here are attempting to distinguish a class of cyclones, cyclops, from other cyclonic storms by the~~ir~~ physics _of their development_, not by the regions in which they develop. Here we present a case of an actual tropical cyclone in the Mediterranean that we do not identify as a cyclop.

4.1 Cyclone Zorbas

The cyclone known as Zorbas developed just north of Libya on 27 September 2018 and moved northward and then northeastward across the Peloponnese and the Aegean (Figure 23). dissipating in early October. The storm killed several people and did millions of dollars of damage.

_Figure 23: Track of Cyclone Zorbas, from 27 September through 2 October, 2018.(Image credit: Wikipedia Commons; https://commons.wikimedia.org/wiki/File:Zorbas_2018_track.png)_

The antecedent (actual, not modified) potential intensity distribution, on 26 September, is displayed in Figure 24. In much of the Mediterranean, the potential intensity was typical of tropical warm pools with values approaching 80 ms^{-1}. As with most medicanes, Zorbas was triggered by an upper tropospheric Rossby wave breaking event (Figure 25), but in this case the cold pool aloft only enhanced the existing potential intensity by about 7 ms^{-1} (on September 27th.) In this case, the maximum 400 hPa geopotential perturbation was around 1500 m^{2}s^{-2}, compared to about 2500 m^{2}s^{-2} in the case of Medicane Zeo of 2005. Zorbas was therefore more like a classic case of a tropical cyclone resulting from tropical transition (Bosart and Bartlo, 1991; Davis and Bosart, 2003, 2004) and we might ~~would~~ not describe it as a cyclop. Note that while the approach of the upper-level cyclone did not appreciably alter the potential intensity, it almost certainly humidified the middle troposphere, making genesis somewhat more likely.

Potential Intensity (m/s), 11:00 GMT, 26 September 2018

610
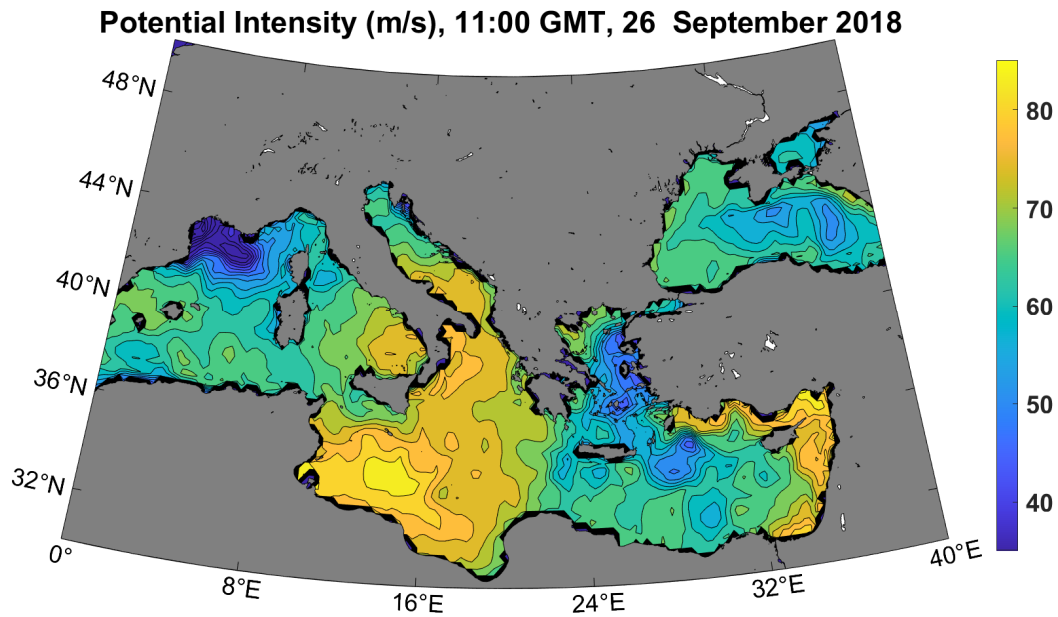
611 *Figure 24: Potential intensity distribution in the Mediterranean and Black Seas, 11 ~~GMT~~UTC on 26 September 2018.*

612

9/26 9/27

613
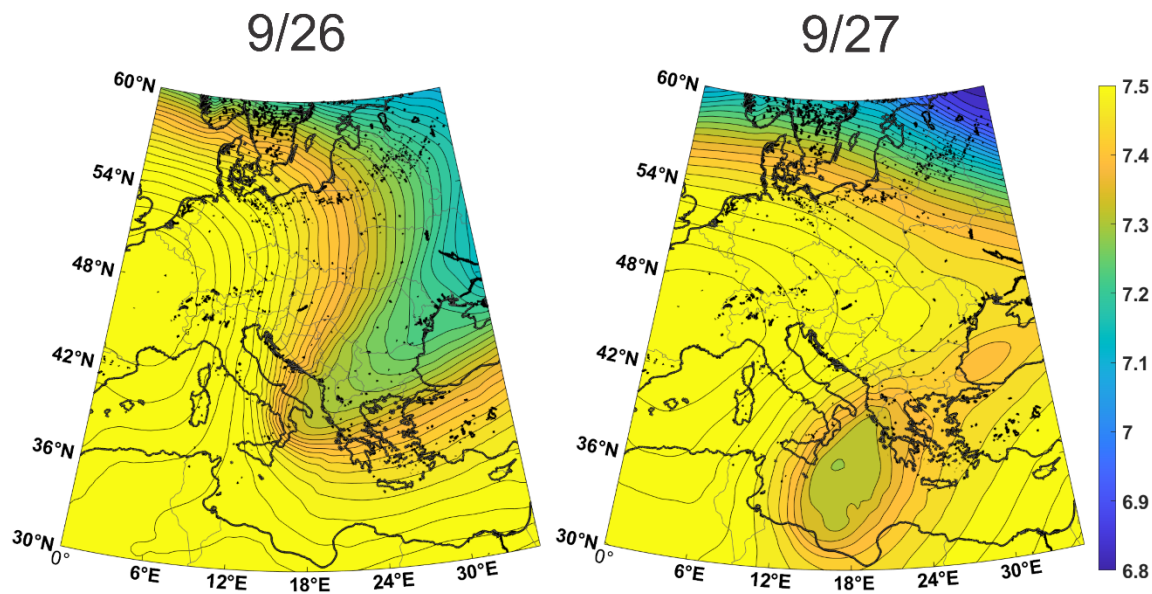
614 *Figure 25: 400 hPa geopotential height (km) at 11 ~~GMT~~UTC on 26 September (left) and 27 September (right), 2018.*
615 *Contour interval is 13.34 m. From ERA-5 reanalysis.*

616 ### 4.2 Cyclone Daniel

617 Cyclone Daniel of 2023 was the deadliest Mediterranean surface flux-driven cyclone in recorded
618 history, with a death toll exceeding 4,000 and thousands of missing persons, mostly owing to
619 floods caused by the catastrophic failure of two dams near Derna, Libya (Flaounas et al., 2024).
620 This flooding was the worst in the recorded history of the African continent. Figure 26 shows the

621 track of Daniel's center and a visible satellite image of the storm as it approached landfall in
622 Libya is shown in Figure 27. Daniel became a surface flux-driven cyclone off the west coast of
623 the Peloponnese on September 5th, made landfall near Benghazi, Libya, on September 10th and
624 dissipated over Egypt on the 12th.

625

Figure 26: Track of Storm Daniel at 6-hour intervals, beginning September 5th and ending September 12th, 2023. The
circles, squares and triangles along the track denote tropical cyclone, subtropical cyclone and extratropical cyclone
designations, respectively, while the deep blue and light blue colors denote tropical depression- and tropical storm-
force winds. (Image credit: Wikipedia commons; https://commons.wikimedia.org/wiki/File:Daniel_2023_track.png)

630
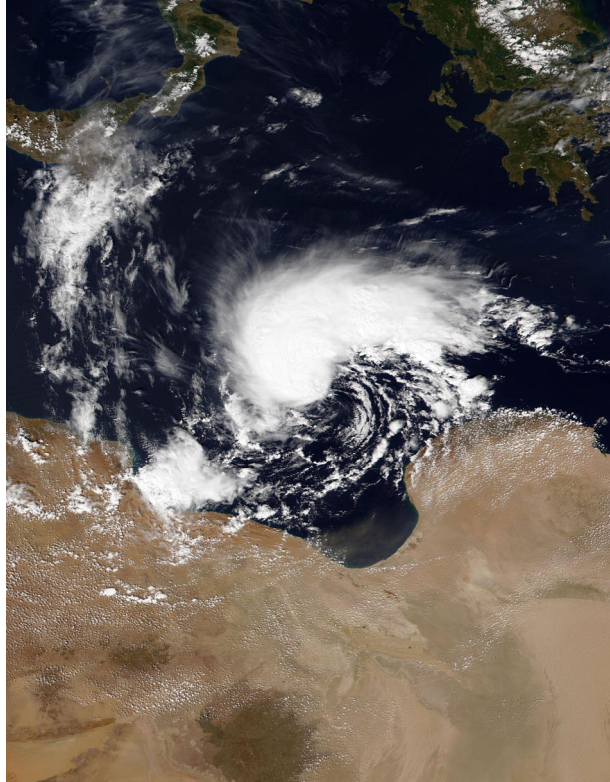
631 *Figure 27: NOAA-20 VIIRS image of Storm Daniel at 12 ~~GMT~~UTC 9 September 2023, as it approached the Libyan*
632 *coast.*

633

634 As with Zorbas, the antecedent potential intensity was high throughout the Mediterranean south
635 and east of Italy and Sicily, and the event was triggered by a Rossby wave breaking event
636 (Figure 28). And as with Zorbas, the cutoff cyclone aloft was not strong enough to appreciably
637 alter the existing potential intensity but acted as a trigger for the tropical cyclone that Daniel
638 became. This was another classic case of tropical transition, and not a cyclop.

639
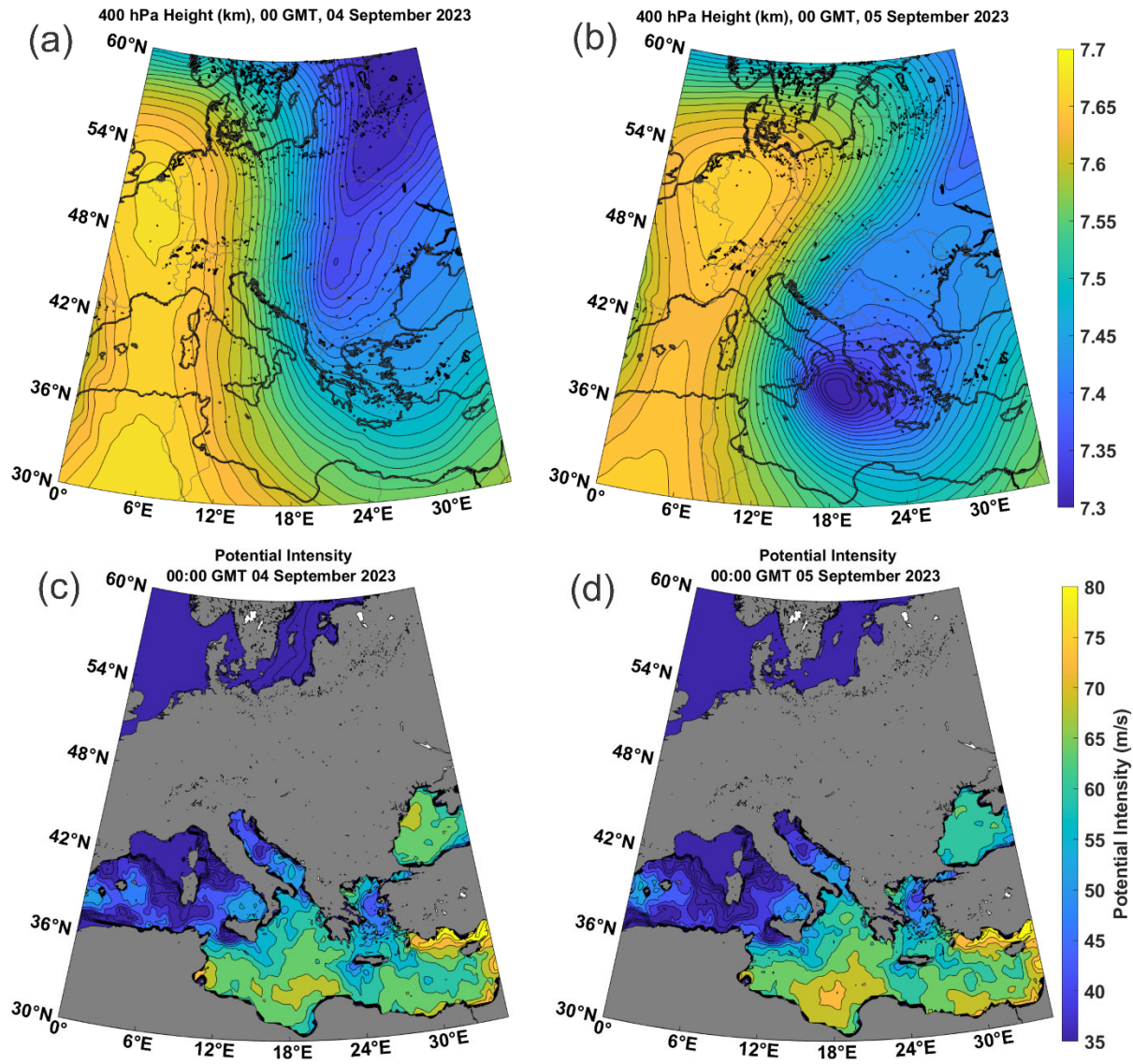
Figure 28: 400 hPa geopotential height (km) with contour interval of 13.33 m (a)-(b); and actual potential intensity (ms⁻¹) with contour interval of 4 ms⁻¹ (c)-(d) at 00 ~~GMT~~UTC September 4ᵗʰ ((a) and (c)) and 5ᵗʰ ((b) and (d)), from ERA-5 reanalyses.

643 Yet Storm Daniel differed from Zorbas in one important respect: as it approached the Libyan
644 coast around September 10ᵗʰ, it came under the influence of strong high-level potential vorticity
645 (PV) advection owing to a mesoscale "satellite" PV mass rotating around the ~~principal~~ upper-
646 level cutoff cyclone (Figure 29). The quasi-balanced forcing associated with the superposition of
647 the high-level PV anomaly with the surface-based warm core probably contributed to Daniel's
648 intensification which, remarkably for a surface flux-driven cyclone, continued after landfall
649 (Hewson et al., 2024).
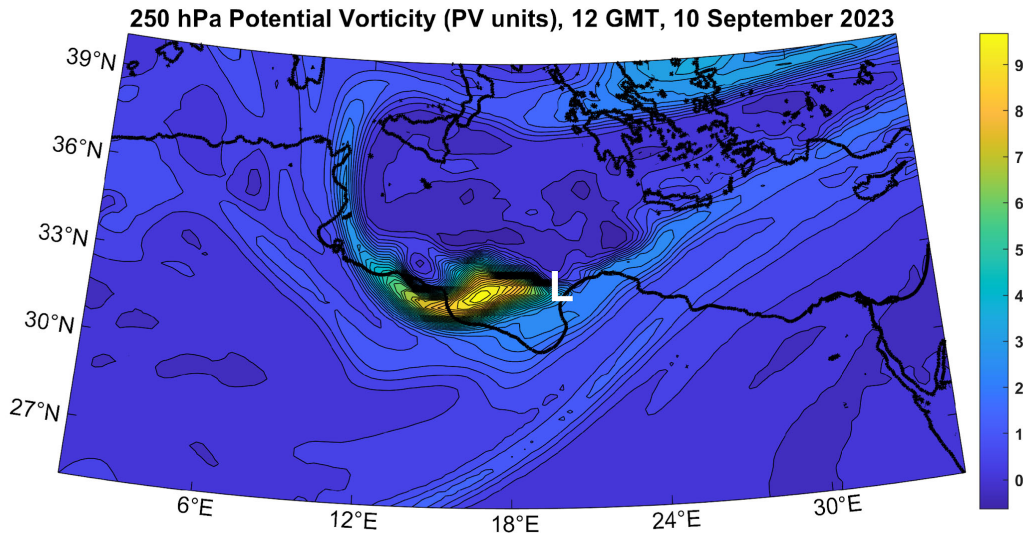
651 *Figure 29: Potential vorticity (PV units, 10^{-6} K kg^{-1} m^2 s^{-1}) at 250 hPa at 12 ~~GMT~~UTC on 10 September, 2023. The*
652 *white "L" marks the approximate surface center of Daniel at this time.*

5. Summary and conclusions

655 We here argue that many of the cyclonic storms called medicanes, polar lows, subtropical
656 cyclones, and Kona storms operate on the same physics and ought to be identified as a single
657 class of storms that we propose to call cyclops. In their developed structure and intensity they
658 are essentially identical to tropical cyclones, and lke TCs ~~Like classical tropical cyclones, these~~
659 are driven primarily by wind-dependent surface enthalpy (latent and sensible heat) fluxes, but
660 unlike classical TCs, there is little or no climatological potential intensity for the storms. Rather,
661 the development and/or migration over relatively warm water approach of strong, cold-core
662 cyclones in the upper troposphere cools and moistens the column through dynamical lifting,
663 generating mesoscale to synoptic scale columns with elevated potential intensity and humidity,
664 and reduced wind shear – ideal embryos for the development of surface flux-driven cyclones.

665 We do not expect cyclops to last as long as classical TCs. In the first place, the conditions that
666 enable such storms are confined in space and transient in time. For example, the cutoff cyclone
667 aloft is often re-absorbed into the main baroclinic flow. In addition, the strong surface enthalpy
668 fluxes that power cyclops also increase, through the action of deep convection, the enthalpy of
669 the otherwise spatially limited cold columns in which they form, reducing over time the
670 thermodynamic disequilibrium between the air column and the sea surface. A back-of-the-
671 envelope estimate for the time to destroy the initial thermodynamic disequilibrium is on the order
672 of days. By contrast, even the strongest classical TCs do not sufficiently warm the large
673 expanses of the tropical troposphere they influence to appreciably diminish the large-scale
674 potential intensity of tropical warm pools.

675 Not all cyclonic storms that have been called polar lows, medicanes, subtropical cyclones, or
676 Kona storms meet our definition of cyclop. The literature describes many polar lows that have
677 been traced to something more nearly like classical baroclinic instability acting in an air mass of
678 anomalously low static stability (e.g. Sardie and Warner, 1985). Many storms identified as Kona
679 storms because of their location and season, and which developed under cold cyclones aloft,
680 never received much of a boost from surface fluxes and therefore would not be classified as
681 cyclops. And, as we described in the last section, two strong Mediterranean cyclones, Zorbas of
682 2018 and Daniel of 2023, developed in environments of high climatological potential intensity
683 and formed via the tropical transition process.

684 Beyond these caveats, not all cold-core, closed cyclones in the upper troposphere that develop
685 or move over relatively warm ocean waters develop cyclops. Without doing a comprehensive
686 survey, we have found several cases of greatly enhanced potential intensity under cold lows
687 aloft that did not develop strong, concentrated surface cyclones. We suspect that, as with
688 classical tropical cyclones, dry air incursions above the boundary layer may have prevented
689 genesis in these cases, but as these events generally occur in regions devoid of in-situ
690 observations, it is not clear how well reanalyses capture variations of moisture on the scale of
691 cyclops. In any event, the efficiency with which upper-level cut-off cyclones produce cyclops,
692 given a substantial perturbation in potential intensity, should be a subject of future research.

693 Clearly, there exists a continuum between pure tropical transition, in which synoptic-scale
694 dynamics play no role in setting up the potential intensity, and pure cyclops in which synoptic-
695 scale processes create all the potential intensity that drives the storm. The distinction we are
696 making here does not pertain to the final result – a tropical cyclone[5] – but to the route to
697 creating it. As a practical matter, We might think of a triangular phase space in which the
698 vertices are pure baroclinic cyclones, pure tropical cyclones, and cyclops, with real storms
699 migrating through that phase space over time, as in phase-space diagrams of (Hart, 2003). This
700 proposed phase space is illustrated in Figure 30. Figure 30: Proposed phase space for
701 baroclinic cyclones, tropical cyclones, and cyclops. AT the lower left corner, pure baroclinic
702 cyclones are driven by ambient baroclinity. At the upper corner, pure tropical cyclones are
703 driven by ambient potential intensity (PI) arising from the thermodynamic disequilibrium between
704 the ocean and atmosphere. At the lower right corner, pure CYCLOPs are driven by PI locally
705 generated by synoptic scale dynamical processes, in the absence of climatological PI. As with
706 Hart's cyclone phase space (Hart, 2003), individual cyclones can migrate through this space
707 over time. Synoptic scale processes, like Rossby wave breaking, are essential not only for
708 triggering cyclops but for providing conducive thermodynamic and kinematic environments for
709 their development. As such, forecasters must account for should consider both the triggering
710 potential and mesoscale to synoptic scale environmental development in predicting the
711 formation and evolution of cyclops. The modified potential intensity (V_{pm}) introduced here may

---

[5] It might be beneficial to develop a term that generically denotes a cyclone driven primarily by surface enthalpy fluxes. "Tropical cyclone" seem unsuited to the task, since "tropical" hardly describes, e.g., a polar low. Such a generic term would encompass both conventional tropical cyclones, which occur in regions of climatologically large potential intensity, and cyclops, for which potential intensity is generated locally in space and time.

712   prove to be a valuable diagnostic that can easily be calculated from NWP model output. To
713   simulate cyclops, NWP models need to make accurate forecasts of ~~baroclinic~~ dynamic
714   processes that lead to the formation and humidification of deep cold pools aloft, and be able to
715   handle surface fluxes and other boundary layer processes essential to the formation of surface
716   flux-driven cyclones. And, as with tropical cyclones, coupling to the ocean is essential for
717   accurate intensity prediction.

718   Finally, we encourage researchers to focus on the essential physics of cyclop developments
719   regardless of where in the world they occur. Casting a broader geographical net will harvest a
720   greater sample of such storms and should lead to more rapid progress in understanding and
721   forecasting them.

722

Appendix

724   Potential intensity is a measure of the maximum surface wind speed that can be achieved by a
725   cyclone fueled entirely by surface enthalpy fluxes. It is defined (see Rousseau-Rizzi and
726   Emanuel (2019) for an up-to-date definition):

727
$$V_p^2 = \frac{C_k}{C_D}\frac{T_s - T_o}{T_o}\left(h_0^* - h_b\right), \qquad (A1)$$

728   Where C_k and C_D are the surface exchange coefficients for enthalpy and momentum, T_s and

729   T_o are the absolute temperatures of the surface and outflow layer, h_0^* is the saturation moist

730   static energy of the sea surface, and h_b is the moist static energy of the boundary layer.

731   Using the relation $T\delta s \simeq \delta h$, where s is moist entropy, we can re-write (A1) slightly as

732
$$V_p^2 = \frac{C_k}{C_D}\frac{T_s - T_o}{T_o}T_s\left(s_0^* - s_b\right). \qquad (A2)$$

733   Next, we assume that the troposphere near cyclops has a nearly moist adiabatic lapse rate[6],
734   and the moist entropy of the boundary layer is equal to the saturation moist entropy, s^*, of the
735   troposphere; i.e., that the troposphere is neutrally stable to moist adiabatic ascent from the
736   boundary layer. Under these conditions, (A2) may be re-written

---

[6] If the lapse rate is appreciably sub-adiabatic, then convection cannot occur and no flux-driven cyclone
could develop. This condition would be associated with a larger value of s* in (A3), which would at last
reduce the calculated value of V_p. Super-adiabatic lapse rates are not generally observed over the ocean
within deep humid layers.

737
$$V_p^2 = \frac{C_k}{C_D} \frac{T_s - T_o}{T_o} T_s \left(s_0^* - s^* \right). \tag{A3}$$

738 Here s^* is constant with altitude, since the troposphere is assumed to have a moist adiabatic
739 lapse rate.

740 Referring to Figure 1a in the main text, we want to know what the potential intensity is ~~under~~ in
741 the vicinity of the cutoff cyclone aloft *before* the atmosphere underneath it has started to warm
742 up under the influence of surface enthalpy fluxes. But in reality, this warming commences as
743 soon as the system moves over relatively warm water. We can infer what the temperature, or
744 s^*, is under the cutoff cyclone by relating the temperature perturbation under the cyclone to the
745 geopotential perturbation associated with the cutoff low.

746 We begin with the perturbation hydrostatic equation in pressure coordinates:

747
$$\frac{\partial \phi'}{\partial p} = -\alpha', \tag{A4}$$

748 where ϕ' is the perturbation geopotential and α' is the perturbation specific volume. Since the
749 latter is a function of pressure and s^* only, we can use the chain rule and one of the Maxwell
750 relations from thermodynamics (Emanuel, 1994) to write (A4) as

751
$$\frac{\partial \phi'}{\partial p} = -\left(\frac{\partial T}{\partial p} \right)_{s^*} s^{*'}. \tag{A5}$$

752 Now, since $s^{*'}$ does not vary with altitude, we can integrate (A5) from the surface to the local
753 tropopause to yield

754
$$\phi_{cl}' - \phi_s' = \left(T_s - T_o \right) s^{*'}. \tag{A6}$$

755 where ϕ_{cl}' is the geopotential perturbation associated with the cutoff cyclone aloft and ϕ_s' is the
756 near-surface geopotential perturbation.

757 We want to know how cold the air is under the cutoff low *before* the surface pressure has
758 dropped, so we can use (A6) to find the temperature (or s^*) perturbation that would be found
759 under the cutoff cyclone in the absence of a surface pressure perturbation:

760
$$s^{*'} = \frac{\phi_{cl}'}{T_s - T_o}. \tag{A7}$$

761 Using this, the modified definition of potential intensity, V_{pm}, can be written from (A1) as

$$V_{pm}^2 = \frac{C_k}{C_D} \frac{T_s - T_o}{T_o} T_s \left(s_0^* - s_e^* - \frac{\phi_{cl}{}'}{T_s - T_o} \right), \tag{A8}$$

763   or equivalently,

$$V_{pm}^2 = V_p^2 - \frac{C_k}{C_D} \frac{T_s}{T_o} \phi_{cl}{}', \tag{A9}$$

765   where V_p is the unperturbed potential intensity, and s_e^* is the unperturbed environmental

766   saturation entropy. We use (A9) in the calculations reported in this paper, with V_p calculated

767   using the algorithm of Bister and Emanuel (2002).

768   For the purposes of the present work, we defined the perturbation as the difference between the
769   actual geopotential and its climatological value determined from monthly mean values over the
770   period 1979-2023, and we estimate the cutoff cyclone geopotential perturbation at 400 hPa.

Code and data availability

772   No modeling was performed in the course of this work, and no code developed except to plot
773   reanalysis data. Routines for calculating potential intensity are available at
774   https://github.com/dgilford/tcpyPI . All of the meteorological analyses presented herein are
775   based in ERA5 downloaded from the Copernicus Climate Change Service
776   (https://doi.org/10.24381/cds.143582cf, Hersbach et al., 2020).

Author contributions

778   KE carried out the analyses and prepared the manuscript with contributions from all the co-
779   authors. JJG prepared Figure 30.

Competing interests

781   The authors declare that they have no conflict of interest.

Acknowledgements

783   We thank two anonymous reviewers for most helpful and conscientious reviews, and Lance
784   Bosart for his detailed and highly constructive comments.

785   This paper was motivated by discussions at the TROPICANA (TROPIcal Cyclones in
786   ANthropocene: physics, simulations & Attribution) program, which took place in June 2024 at
787   the Institute Pascal, University of Paris-Saclay, and aimed to address complex issues related to
788   tropical cyclones, medicanes, and their connection with climate change.

789   This work was made possible by Institut Pascal at Université Paris-Saclay with the support of
790   the program TROPICANA, "Investissements d'avenir" ANR-11-IDEX-0003-01.

791   T.Alberti acknowledges useful discussions within the MedCyclones COST Action (CA19109)
792   and the FutureMed COST Action (CA22162) communities.

793   S. Bourdin received financial support from the NERC-NSF research grant n° NE/W009587/1
794   (NERC) & AGS-2244917 (NSF) HUrricane Risk Amplification and Changing North Atlantic
795   Natural disasters (Huracan), and from the EUR IPSL-Climate Graduate School through the
796   ICOCYCLONES2 project, managed by the ANR under the "Investissements d'avenir"
797   programme with the reference 37 ANR-11-IDEX-0004 - 17-EURE-0006.

798   S.J. Camargo and C.-Y. Lee acknowledge the support of the U.S. National Science Foundation
799   (AGS 20-43142, 22-17618, 22-44918) and U.S. Department of Energy (DOE) (DE-
800   SC0023333).

801   K. Emanuel was supported by the U.S. National Science Foundation under grant AGS-2202785.

802   M. M. Miglietta was partly supported by "Earth Observations as a cornerstone to the
803   understanding and prediction of tropical like cyclone risk in the Mediterranean (MEDICANES)",
804   ESA Contract No. 4000144111/23/I-KE.

805   H. Ramsay acknowledges funding support from the Climate Systems Hub of the Australian
806   Government's National Environmental Science Program (NESP).

807   R. Romero acknowledges financial support by the "Ministerio de Ciencia e Innovación" of Spain
808   through the grant TRAMPAS (PID2020-113036RB-I00/AEI/10.13039/501100011033).

809

References

811   Bister, M. and Emanuel, K. A.: Low frequency variability of tropical cyclone potential intensity, 1:
812   Interannual to interdecadel variability, J Geophys Res, 107, doi:10.1029/2001JD000776, 2002.

813   Bosart, L. F. and Bartlo, J. A.: Tropical storm formation in a baroclinic environment, Mon Wea
814   Rev, 119, 1979–2013, 1991.

815   Cangliosi, J. P., Papin, P., and Beven, J. L.: Unnamed tropical storm (AL012023)., 2023.

816   Cavicchia, L., von Storch, H., and Gualdi, S.: A long-term climatology of medicanes, Clim. Dyn.,
817   43, 1183–1195, https://doi.org/10.1007/s00382-013-1893-7, 2014.

818   Cavicchia, L., Pepler, A., Dowdy, A., and Walsh, K.: A physically based climatology of the
819   occurrence and intensification of Australian East Coast Lows, J. Clim., 32, 2823–2841,
820   https://doi.org/10.1175/JCLI-D-18-0549.1, 2019.

821   Chavas, D. R. and Emanuel, K. A.: Equilibrium tropical cyclone size in an idealized state of
822   axisymmetric radiative–convective equilibrium, J Atmos Sci, 71, 1663–1680, 2014.

823   Cronin, T. W. and Chavas, D. R.: Dry and semidry tropical cyclones, J. Atmospheric Sci., 76,
824   2193–2212, https://doi.org/10.1175/jas-d-18-0357.1, 2019.

825   Daingerfield, L. H.: Kona storms, Mon. Weather Rev., 49, 327–329,
826   https://doi.org/10.1175/1520-0493(1921)49<327:ks>2.0.co;2, 1921.

827   Davis, C. A. and Bosart, L. F.: Baroclinically induced tropical cyclogenesis, Mon. Weather Rev.,
828   131, 2730–2747, https://doi.org/10.1175/1520-0493(2003)131<2730:BITC>2.0.CO;2, 2003.

829   Davis, C. A. and Bosart, L. F.: The TT problem: Forecasting the tropical transition of cyclones,
830   Bull. Am. Meteorol. Soc., 85, 1657–1662, https://doi.org/10.1175/BAMS-85-11-1657, 2004.

831   Emanuel, K.: Genesis and maintenance of "Mediterranean hurricanes," Adv Geosci, 2, 217–
832   220, 2005.

833   Emanuel, K.: Tropical cyclone activity downscaled from NOAA-CIRES reanalysis, 1908-1958, J
834   Adv Model Earth Sys, 2, 1–12, 2010.

835   Emanuel, K. A.: Atmospheric Convection, Oxford Univ. Press, New York, 580 pp., 1994.

836   Emanuel, K. A.: Some aspects of hurricane inner-core dynamics and energetics., J Atmos Sci,
837   54, 1014–1026, 1997.

838   Emanuel, K. A., Neelin, J. D., and Bretherton, C. S.: On large-scale circulations in convecting
839   atmospheres, Quart J Roy Meteor Soc, 120, 1111–1143, 1994.

840   Evans, J. L. and Braun, A.: A climatology of subtropical cyclones in the South Atlantic, J. Clim.,
841   25, 7328–7340, https://doi.org/10.1175/JCLI-D-11-00212.1, 2012.

842   Fita, L. and Flaounas, E.: Medicanes as subtropical cyclones: the December 2005 case from
843   the perspective of surface pressure tendency diagnostics and atmospheric water budget, Q. J.
844   R. Meteorol. Soc., 144, 1028–1044, https://doi.org/10.1002/qj.3273, 2018.

845   Flaounas, E., Dafis, S., Davolio, S., Faranda, D., Ferrarin, C., Hartmuth, K., Hochman, A.,
846   Koutroulis, A., Khodayar, S., Miglietta, M. M., Pantillon, F., Patlakas, P., Sprenger, M., and
847   Thurnherr, I.: Dynamics, predictability, impacts, and climate change considerations of the
848   catastrophic Mediterranean Storm Daniel (2023), EGUsphere, 2024, 1–29,
849   https://doi.org/10.5194/egusphere-2024-2809, 2024.

850   Gozzo, L. F., Rocha, R. P. da, Reboita, M. S., and Sugahara, S.: Subtropical cyclones over the
851   southwestern South Atlantic: Climatological aspects and case study, J. Clim., 27, 8543–8562,
852   https://doi.org/10.1175/JCLI-D-14-00149.1, 2014.

853   Hersbach, H., Bell, B., Berrisford, P., Hirahara, S., Horányi, A., Muñoz-Sabater, J., Nicolas, J.,
854   Peubey, C., Radu, R., Schepers, D., Simmons, A., Soci, C., Abdalla, S., Abellan, X., Balsamo,
855   G., Bechtold, P., Biavati, G., Bidlot, J., Bonavita, M., De Chiara, G., Dahlgren, P., Dee, D.,

856   Diamantakis, M., Dragani, R., Flemming, J., Forbes, R., Fuentes, M., Geer, A., Haimberger, L.,
857   Healy, S., Hogan, R. J., Hólm, E., Janisková, M., Keeley, S., Laloyaux, P., Lopez, P., Lupu, C.,
858   Radnoti, G., de Rosnay, P., Rozum, I., Vamborg, F., Villaume, S., and Thépaut, J.-N.: The
859   ERA5 global reanalysis, Q. J. R. Meteorol. Soc., 146, 1999–2049,
860   https://doi.org/10.1002/qj.3803, 2020.

861   Hewson, T., Ashoor, A., Bousetta, S., Emanuel, K., Lagouvardos, K., Lavers, D., Magnusson,
862   L., Pillosu, F., and Zoster, E.: Medicane Daniel: an extraordinary cyclone with devastating
863   impacts, ECMWF Newsl., 179, 33–47, 2024.

864   Holland, G. J., Lynch, A. H., and Leslie, L. M.: Australian east-coast cyclones. Part I: Synoptic
865   overview and case study, Mon. Weather Rev., 115, 3024–3036, https://doi.org/10.1175/1520-
866   0493(1987)115<3024:AECCPI>2.0.CO;2, 1987.

867   McIntyre, M. E. and Palmer, T. N.: Breaking planetary waves in the stratosphere, Nature, 305,
868   593–600, https://doi.org/10.1038/305593a0, 1983.

869   McTaggart-Cowan, R., Deane, G. D., Bosart, L. F., Davis, C. A., and Galarneau, T. J.:
870   Climatology of tropical cyclogenesis in the North Atlantic (1948–2004), Mon. Weather Rev., 136,
871   1284–1304, https://doi.org/10.1175/2007MWR2245.1, 2008.

872   McTaggart-Cowan, R., Galarneau, T. J., Bosart, L. F., Moore, R. W., and Martius, O.: A global
873   climatology of baroclinically influenced tropical cyclogenesis, Mon. Weather Rev., 141, 1963–
874   1989, https://doi.org/10.1175/MWR-D-12-00186.1, 2013.

875   McTaggart-Cowan, R., Davies, E. L., Fairman, J. G., Galarneau, T. J., and Schultz, D. M.:
876   Revisiting the 26.5°c sea surface temperature threshold for tropical cyclone development, Bull.
877   Am. Meteorol. Soc., 96, 1929–1943, https://doi.org/10.1175/BAMS-D-13-00254.1, 2015.

878   Miglietta, M. M. and Rotunno, R.: Development mechanisms for Mediterranean tropical-like
879   cyclones (medicanes), Q. J. R. Meteorol. Soc., 145, 1444–1460, https://doi.org/10.1002/qj.3503,
880   2019.

881   Nastos, P. T., Karavana Papadimou, K., and Matsangouras, I. T.: Mediterranean tropical-like
882   cyclones: Impacts and composite daily means and anomalies of synoptic patterns, High Impact
883   Atmospheric Process. Mediterr., 208, 156–166, https://doi.org/10.1016/j.atmosres.2017.10.023,
884   2018.

885   Nordeng, T. E. and Rasmussen, E. A. D.-:10. 1034/j. 1600-0870. 1992. 00001. x: A most
886   beautiful polar low. A case study of a polar low development in the Bear Island region, Tellus A,
887   44, 81–99, 1992.

888   Otkin, J. A. and Martin, J. E.: A synoptic climatology of the subtropical Kona storm, Mon.
889   Weather Rev., 132, 1502–1517, https://doi.org/10.1175/1520-
890   0493(2004)132<1502:ASCOTS>2.0.CO;2, 2004.

891   Pytharoulis, I., Craig, G. C., and Ballard, S. P.: Study of the Hurricane-like Mediterranean
892   cyclone of January 1995, Phys. Chem. Earth Part B Hydrol. Oceans Atmosphere, 24, 627–632,
893   https://doi.org/10.1016/S1464-1909(99)00056-8, 1999.

894 Romero, R. and Emanuel, K. D.-:10. 1002/jgrd. 50475: Medicane risk in a changing climate, J
895 Geophys Res, 118, 2013.

896 Rotunno, R. and Emanuel, K. A.: An air-sea interaction theory for tropical cyclones. Part II., J
897 Atmos Sci, 44, 542–561, 1987.

898 Rousseau-Rizzi, R. and Emanuel, K.: An evaluation of hurricane superintensity in axisymmetric
899 numerical models, J. Atmospheric Sci., 76, 1697–1708, https://doi.org/10.1175/jas-d-18-0238.1,
900 2019.

901 Sardie, J. M. and Warner, T. T. D.-:10. 1111/j. 1600-0870. 1985. tb00444. x: A numerical study
902 of the development mechanisms of polar lows, Tellus A, 37A, 460–477, 1985.

903 Simpson, R. H.: Evolution of the Kona storm: A subtropical cyclone, J. Atmospheric Sci., 9, 24–
904 35, https://doi.org/10.1175/1520-0469(1952)009<0024:EOTKSA>2.0.CO;2, 1952.

905 Tomita, H. and Tanaka, R.: Ocean surface warming and cooling responses and feedback
906 processes associated with polar lows over the Nordic seas, J. Geophys. Res. Atmospheres,
907 129, e2023JD040460, https://doi.org/10.1029/2023JD040460, 2024.

908 Tous, M. and Romero, R. D.-:10. 1002/joc. 3428: Meteorological environments associated with
909 medicane development, Int. J. Climatol., 33, 1–14, 2013.

910 Velez-Pardo, M. and Cronin, T. W.: Large-scale circulations and dry tropical cyclones in direct
911 numerical simulations of rotating Rayleigh-Bénard convection, J. Atmospheric Sci.,
912 https://doi.org/10.1175/JAS-D-23-0018.1, 2023.

913 Yanase, W. and co-authors: Climatology of polar lows over the Sea of Japan using the JRA-55
914 reanalysis, J Clim., 29, 419–437, 2016.

915 Yarovaya, D. A., Efimov, V. V., Shokurov, M. V., Stanichnyi, S. V., and Barabanov, V. S.: A
916 quasitropical cyclone over the Black Sea: Observations and numerical simulation, Phys.
917 Oceanogr., 18, 154–167, https://doi.org/10.1007/s11110-008-9018-2, 2008.

918 Zhang, W., Villarini, G., Scoccimarro, E., and Napolitano, F.: Examining the precipitation
919 associated with medicanes in the high-resolution ERA-5 reanalysis data, Int. J. Climatol., 41,
920 E126–E132, https://doi.org/10.1002/joc.6669, 2021.

921 Zhang, Y., Meng, Z., Zhang, F., and Weng, Y.: Predictability of tropical cyclone intensity
922 evaluated through 5-yr forecasts with a convection-permitting regional-scale model in the
923 Atlantic basin, Wea Forecast., 29, 1003–1022, 2014.

924